DYNAMICS OF A PET WEB IN A ROLL-TO-ROLL SYSTEM

BY

MURAD ALI

A Thesis Presented to the
DEANSHIP OF GRADUATE STUDIES

KING FAHD UNIVERSITY OF PETROLEUM & MINERALS
DHAHRAN, SAUDI ARABIA

In Partial Fulfillment of the
Requirements for the Degree of

MASTER OF SCIENCE

In

MECHANICAL ENGINEERING

MAY 2016

KING FAHD UNIVERSITY OF PETROLEUM & MINERALS
DHAHRAN 31261, SAUDI ARABIA

DEANSHIP OF GRADUATE STUDIES

This thesis, written by **MURAD ALI** under the direction of his thesis advisor and approved by his thesis committee, has been presented to and accepted by the Dean of Graduate Studies, in partial fulfillment of the requirements for the degree of **MASTER OF SCIENCE IN MECHANICAL ENGINEERING**.

Thesis Committee

Dr. Muhammad Hawwa (Advisor)

Dr. Zuhair M. Gasem
Department Chairman

Dr. Sulaiman Pashah (Member)

Dr. Salam A. Zummo
Dean of Graduate Studies

Dr. Mahir Hassan (Member)

29/5/16
Date

Dedicated

To my parents and siblings
for their unconditional support and trust.

ACKNOWLEDGEMENTS

First and foremost, I would like to thank almighty Allah (SWT).

I would like to express my appreciation and sincere thanks to my advisor Dr. Muhammad Hawwa for his guidance and support throughout my thesis work. Throughout my simulations and experimental work, he provided encouragement, good teaching and lot of good ideas.

I would like to thank again to my advisor who provided me an opportunity to visit Massachusetts Institute of Technology (USA) for one semester to perform my experimental work. I am also grateful to Professor. David Hardt, who supported me during my visit and his meetings, suggestions and recommendations made my work valuable. I would like to thank Dr. Xian Du and Aalim Mustafa, they helped me during my experimental work and their good ideas, and tough questions helped me a lot to learn new things.

I am very thankful to my Thesis Committee Members; Dr. Sulaiman Pasha and Dr. Mahir Hassan for their precious comments, valuable suggestions and technical support.

I would like to acknowledge King Fahd University of Petroleum and Minerals for giving me an opportunity to pursue MS degree at Mechanical engineering

department and I would also appreciate Deanship of Research at King Fahd University of Petroleum and Minerals for funding my MS project under research grant #. MIT13101/02.

An acknowledgment would not be complete without appreciating my mother, my brothers and my sister, for their continuous prayers and encouragement. Finally, I would like to thank Muhammad Yasir Khan, Muhammad Azhar Ali Khan, Syed Abdul Salam and Ihsanullah.

TABLE OF CONTENTS

LIST OF TABLES

LIST OF FIGURES

LIST OF ABBREVIATIONS

ϵ	Nonlinear strain
η	Dynamic viscosity of the dash-pot
μ	Air damping coefficient
ν	Poisson's ratio
ω	Angular frequency
ρ	Web density
ρ_l	Mass per unit length
ρ_v	Mass per unit volume
$\sigma(x,t)$	Longitudinal stress
A	Cross-sectional area of the string
a	Harmonic coefficient
A_m	Amplitude of excitation
A_r	Cross-sectional area of the string
E	Modulus of elasticity
f	Natural frequency
$K.E$	Kinetic energy
L	Web length

P	Applied constant axial force
$P.E$	Potential energy
v	Constant axial speed
$V.W$	Virtual work
$w(x,t)$	Transverse vibration
$w_{,t}$	Transverse speed

THESIS ABSTRACT

NAME: Murad Ali

TITLE OF STUDY: Dynamics of a PET web in a roll-to-roll system

MAJOR FIELD: Mechanical Engineering

DATE OF DEGREE: May, 2016

In roll-to-roll manufacturing systems, a continuous web is passed through processing machinery to obtain a final product. During processing, different kinds of operations are carried out such as printing, coating, lamination, etc. The web, also called substrate, can take the form of thin film, belt, paper, rubber, strip, foil, fabric, etc. Many of the products can be obtained in their rolled form, like newspaper, metal sheets, and plastics. This roll-to-roll system is utilized for mass production within an automated environment. The purpose of this study is to investigate Polyethylene terephthalate (PET) thin film web dynamics of a roll-to-roll system used in micro-contacting printing applications. The purpose is to establish a mathematical model based on axially moving string in the form of nonlinear differential equations to find the relationship among web frequency, axial speed and tension. Kelvin-Voight viscoelastic model is introduced into the equation of motion and, analytical and numerical simulations are

carried out in Mathematica and Comsol respectively to investigate the string model. The effect of web tension, axial speed, air damping and dynamic viscosity on the time history response of the system is analyzed using Galerkin's numerical approximation and found that web axial speed, air damping and dynamic viscosity has no significant effect as compared to the web tension, while air damping and dynamics viscosity minimize the amplitude of time history response. The viscoelastic properties of PET (creep and relaxation) are investigated at room temperature, thus confirming its viscoelastic behavior in ambient conditions. The analytical relationship among web axial speed, transmitted tension and frequency is found from string model, which shows that web vibration frequency is strongly affected by web tension as compared to web axial speed and in fact web axial speed has negligible effect on the web vibration frequency. Numerical simulations for string model are carried out in Comsol, finding that web vibration frequency is strongly affected by web transmitted tension as compared to the web axial speed, thus validating analytical string model. A new displacement sensor is utilized in this study to measure web transverse vibration. A Fast Fourier Transform (FFT) algorithm is applied to web transverse displacement measured by displacement sensor, to find the experimental relationship among web axial speed, transmitted tension and vibration frequency. Based on FFT analysis it is found that web transmitted tension has strong effect on the web vibration frequency and results are found in good agreement with the analytical string model ones, while experimental results show stronger effect of web axial speed on web vibration frequency than the analytical string model ones.

MASTER OF SCIENCE

KING FAHD UNIVERSITY OF PETROLEUM AND MINERALS

Dhahran 31261, Saudi Arabia

ملخص الرسالة

الاسم مراد علي

عنوان الرسالة ديناميكا شريط تتراهالايد بولي إيثيلين في نظام ثنائي اللف

التخصص الهندسة الميكانيكة

تاريخ التخرج أيار، 2016

في نظم اللف الثنائي التصنيعية، يمرر شريط (سير) مستمر خلال آلية المعالجة للحصول على منتج نهائي. أثناء عملية المعالجة ، يتم تنفيذ أنواع مختلفة من العمليات مثل، الطباعة، التغليف، الطلاء، التصفيح، ... إلخ . الشريط، ويسمى أيضا الطبقة، يمكن أن يأخذ شكل طبقة رقيقة، سير، ورقة، مطاط، صفيحة، قماش، إلخ. كثير من المنتجات يمكن الحصول عليها في شكلها الملفوف، مثل الجرائد، الصفائح المعدنية، والمواد البلاستيكية. يستخدم هذا النظام ثنائي اللف للإنتاج بكميات كبيرة ضمن بيئة أتوماتيكية. الغرض من هذه الدراسة هو بحث وإستقصاء ديناميكا و حركة شريط تتراهالايد بولي إيثيلين رقيق في نظام ثنائي اللف مستخدم في تطبيقات الطباعة باستخدام التلامس الدقيق. يهدف البحث إلى تأسيس نموذج رياضي مبنيٌ على نموذج خيط متحرك أفقيا في شكل معادلات تفاضلية لا خطية لإيجاد العلاقة بين تردد الشريط، سرعته الأفقية، والشد في الشريط. نسبةً إلى السلوك التبددي في مثل هذه الآلات، تم تقديم نموزج كلفن-فويت اللزج في المعادلة الحاكمة للحركة وتمت

عمليات المحاكاة في برنامجي ماثيماتيكا و كومسول لدراسة وإستقصاء النموذج الرياضي للشريط. تم تحليل تأثير الشد على الشريط ، سرعته الأفقية ، و تخميد لزوجة الهواء على السجل الزمني لإستجابة النظام بإستخدام تقريب جاليركين و وجد أن السرعة الأفقية و تخميد لزوجة الهواء ليس لهما أثر كبير كتأثير الشد على الشريط، و أن تخميد لزوجة الهواء يقلل من اتساع الأستجابة . تمت دراسة خصائص تتراهالايد بولي إيثيلين اللزجة (الزحف والتليُّن) في درجة حرارة الغرفة. تجريبيا. تم إيجاد العلاقة النظرية بين السرعة الأفقية و الشد على الشريط ، و بين تردد اهتزاز الشريط ، والتي توضح أن التردد يتأثر بصورة كبيرة بالشد مقارنة مع السرعة الأفقية و التي اتضح أن لها تأثير قليل متجاهل. تم الحصول على محاكاة لنموذج الشريط في برنامج كومسول ، وتم بواسطته التحقق و مطابقة النتائج المتحصل عليها من المعادلة النظرية. كذلك، تم استخدام حساس مسافة جديد لقياس اهتزاز الشريط. تم إستخدام خوارزمية تحويل فوريير السريع لإيجاد تردد الشريط وتأثره مع السرعة الأفقية والشد على الشريط باستخدام بيانات الحساس المسجلة. بناءا على تحليل تحويل فوريير السريع وجد أن هناك مقاربة جيدة مع النتائج التحليلة والتجريبية لتأثير شد الشريط على تردده، بينما تُظهر النتائج التجريبية تأثيرا أقوى لسرعة الشريط الأفقية على تردده أكبر من المتحصل عليها في النموزج

ماجستير العلوم

جامعة الملك فهد للبترول والمعادن

الظهران ٣١٢٦١، المملكة العربية السعودية

CHAPTER 1

INTRODUCTION

This chapter is dedicated to the introduction of roll-to-roll systems and micro-contact printing technology. Further, thesis contributions and organization are presented.

1.1 Introduction

In roll-to-roll manufacturing systems, a continuous web is passed through processing machinery and finally a finished product is obtained. During processing, different kinds of operations are carried out, such as printing, coating, lamination, etc. The web, also called substrate can take form of a thin film, belt, paper, rubber, strip, foil, fabric, etc. Many of the products can be obtained in their rolled form, such as newspaper, metal sheets and plastics. This roll-to-roll system is utilized for mass production within an automated environment.

Currently, nanostructures are commonly fabricated using techniques such as photo-lithography, electron-beam writing and X-ray lithography. Although these are proven technologies that provide high-quality outputs but still there are inherent problems. These techniques are generally expensive, slow and the production of large patterns is difficult. Another technology is required that can enable economical manufacturing of nanostructures at high production rates, low cost and good quality.

Micro-contact printing was developed in the early 90's by Whitesides and Kumar

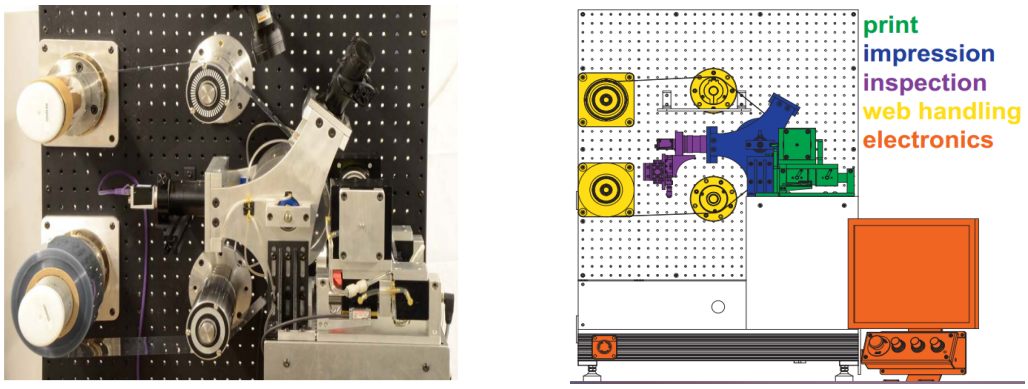

(a) μCP machine (b) subsystem layout

Figure 1.1: Roll-to-roll micro-contact printing (μCP) machine.

[1,2] at Harvard University. Micro-contact printing is a promising technology in which a patterned elastomeric stamp is used to transfer patterns of self-assembled monolayers (SAMs) onto a substrate by conformal contact. It has been demonstrated with a resolution of 30 nm, a minimum feature size of 40 nm and millisecond deposition time. Presently the art remains primarily a research topic but by adapting the technology to new processes makes feasible large scale manufacturing method. Micro-contact printing machine was modified by stagnation in 2008 as shown in Figure 1.1a with all its main parts can be seen. This machine was built by Massachusetts Institute of Technology (MIT) team. This project is funded by the Center for Clean Water and Clean Energy, a joint program between MIT and KFUPM. The layout of all subsystems of μCP machine is presented in Figure 1.1b by Albert [3]. A detailed literature about micro-contact printing, achievements and limitations is available in [4,5].

Web materials during process exhibit vibrations due to structural changes and loading conditions, which can have a great effect on the system dynamics. Web materials are transported at high speeds based on the industrial applications and are more prone to vibrate and become unstable. Vibrations of a web material is of vital importance because it can have severe effect on the production and quality of printing in

roll-to-roll applications. Structural changes which are function of dynamic characteristics like natural frequencies and mode shapes, geometric configuration and material properties cause vibrations. Small irregularities in structures are called mis-tuning and when this combine internally with weak coupling, causing high sensitivity to vibration phenomenon, called localization. Many of the researchers have investigated that even a small degree of mis-tuning have significant effect on vibrations. In this study our main goal is to investigate the effect of these vibrations on dynamic behavior of a roll-to-roll system with PET web, where a single-span simply supported string model is considered for system dynamics analysis.

Micro-contact printing machine is developed by MIT team and the ultimate goal is to get high quality mass production on micron level. To achieve this goal, it is necessary to investigate the dynamics, longitudinal and transverse vibrations of the web in a of roll-to-roll system. But due to the low frequencies of transverse vibration, they are more prone to all small internal or external disturbances. Therefore, a new mathematical model is developed for the transverse vibration measurement of an axially moving elastic and viscoelastic strings.

Dynamics and vibrations of a moving web is a complicated phenomenon and need to be measured. Therefore, proposing and utilizing a proper sensor is an open research area. In the literature researchers have used various approaches to measure web transverse vibration, such as laser, pressure and infra-red sensors by Vedrines et al. [6]. But in our case, a simple USB powered displacement sensor has been used to measure web vibration with a 0.004 mil resolution and 82.6 mil linear range. This leads to the following contributions:

1. A new mathematical model based on axially moving string is developed, linearized and solved analytically to find a solution for transverse vibration and web dynamics response.

2. Kelvin-Voight viscoelastic model is used to introduce viscoelasticity to the axi-

ally moving string.

3. Harmonic Balance Method (HBM) is used for elastic and viscoelastic string models and a relationship among axial speed, tension and frequency of axially moving web is derived. The effect of dynamic viscosity on web frequency and amplitude time history response is investigated.

4. The effect of damping due to air pressure is introduced to the elastic and viscoelastic axially moving string models.

5. Comsol simulations for stationary string and thin plate models are performed to validated web frequency results as compared to the analytical models.

6. A novel displacement sensor based on light triangulation from fiberoptics bundles is utilized to measure web flutter.

7. On experimental data from sensor, Fast Fourier Transform (FFT) algorithm is applied to get web vibration frequency at various web axial speeds and transmitted tensions.

8. Viscoelastic properties of PET such as creep and relaxation at room temperature using Instron 5869 testing machine are investigated.

1.2 Thesis organization

In chapter 1, introduction to micro-contact printing, importance and its history are discussed briefly. In addition to this, thesis contributions and its organization are also discussed at the end of the chapter. In chapter 2, background of axially moving materials, axially moving viscoelastic materials and web transverse vibration measurement are discussed. In chapter 3, PET web characterization of viscoelastic properties at room temperature by using Instron 5869 testing machine are investigating. In

chapter 4, transverse vibrations of axially moving string are investigating analytically. The relationship for dynamic parameters is obtained and Comsol simulations for both string and thin plate models are carried out to validate analytical results. In chapter 5, transverse vibrations are experimentally investigated and displacement sensor is used to measure web flutter and find web frequency by using an FFT algorithm and experimental results are compared with analytical ones obtained in chapter 4. Final concluding remarks are presented and also further recommendations are suggested for possible future work in chapter 6.

CHAPTER 2

BACKGROUND

This chapter is about the literature study of axially moving materials which could be strings, membranes, beams and plates. The main focus is on string model and introducing viscoelasticity bring the discussion of axially moving viscoelastic materials. Furthermore, almost all the previous sensors for web flutter measurement and advantages of the utilized displacement sensor are discussed.

2.1 Axially moving materials

In literature, studies about axially moving materials have been carried out in [7–9]. High transport speeds are attained through webs and their dynamic behavior changes, therefore it is of vital importance to study and understand this behavior. To understand the dynamics and vibrations of these materials, is of great significance in engineering. There are two types of axially moving materials, one is linear [10–13] and other is nonlinear [14–17]. The nonlinear models are difficult to deal analytically but provide much more precise model behavior than linear ones. Web speed is important and affects instability of an axially moving system. It was investigated that speed is not varying with time by Parker [11], where moving string is supported by elastic foundation. This support provide a different stability behavior to axially moving string than the unsupported one. One the other hand, researchers also investigated the

dynamics of such systems with a varying speed and this variation is considered to be small harmonic one. In literature there is very limited work related to the viscoelastic string and most of them are based on beam model. For example, Chen et al. in [18], a viscoelastic beam is considered with a pulsating speed and time invariant response was analyzed with the help of two nonlinear models. In many industrial applications, a number of web materials like polymers, fibers, belts, power transmission chains, magnetic tapes, band saws, pipes for different fluids transportation, metal sheets and papers are considered as axially moving strings materials. For a web to avoid breaking, folding, wrinkling, it must be dynamically stable and not susceptible to vibrations. To understand state of knowledge of these moving materials, K. Marynowski [19] investigated both string and beam like systems . Van Horssen et al. [20] considered axially moving string to be non-homogeneous and its equation was solved by initial boundary value problem. Then non-homogeneity in the equation of motion was due to the external force and velocity of the string was considered to be invariant. It was found the method of Laplace Transform to solve the problem is better than modal analysis.

2.1.1 Axially moving viscoelastic materials

In reality axially moving materials are considered to be energy dissipative mechanisms. Viscoelasticity is an approach discussed by Zhan and Chen [18, 21], to model these dissipative mechanisms. Many of the engineering devices such as paper, magnetic tapes, band saw, polymer and belts can be modeled as axially moving webs. A thin, flat rectangular material having small flexural rigidity is called a web. Webs translation speed varies from applications point of view for example, paper webs goes up to 1968.5 in/sec as compared to 0.1 in/sec in the case of micro-contact printing. Speed variations are very important for stable web operations, therefore, if web goes above the critical speed where web frequency becomes zero, becomes instable in

form of flutter and divergence. With the web axial speed, tension is also an important parameter and its variations effect significantly frequency of transverse vibration. Transverse vibrations are of low frequencies therefore, are more prone to be affected by environmental and machine parameters. These vibrations are of main concern to investigate the dynamics of such systems and if they are completely investigated, then it is easy to apply control strategies for eliminating instabilities. Ghayesh studied analytically [22], nonlinear transverse vibration of a viscoelastic string which is supported by a partial viscoelastic guide. Multiple scales method is implemented to partial differential equations for stability through R-H criterion. Numerical solutions are provided for studying the effect of system parameters on natural frequency, stability conditions and bifurcation points of viscoelastic string model. Chen et al. [23] investigated a computation method and independent functions set is suggested for nonlinear vibrations of axially moving viscoelastic accelerating string. These independent functions convert nonlinear partial differential equations (PDEs) into a set of differential-algebraic equations which can be solved numerically. Zhang et al. [24] analyzed transverse vibration of viscoelastic string by Galerkin method. Galerkin method is applied based on stationary and translating eigenfunction to study both chaotic and regular motion. Based on Poincaré maps, it is concluded numerically that periodic, Quasi-periodic and chaotic motions exist in transverse vibration of such systems. Chen et al. [25] investigated an accelerating viscoelastic string by deriving equation of motion using second law of Newton . The differential-integral equation is solved numerically by Galerkin approximation and the effect of viscosity coefficient and frequency on time history response of the system is investigated.

2.2 Web transverse vibration measurement

In roll-to-roll systems when web moves between rollers an important phenomenon called web flutter (complex oscillatory motion) occurs and it is similar to the motion experienced by flag. The causes of this phenomenon could be air jets exposure, air for drying purposes etc. For a stable web operation, it is important to measure and apply a proper control technique to minimize this flutter. To measure this phenomenon researchers have proposed different sensors such as pressure sensor, laser sensor, infrared sensor, stroboscope, laser vibro-meter and vision based systems [6, 26–33]. An experimental procedure in which a laser sensor detects transverse vibration amplitude, is used to find tension in the web as frequency of free vibration can be found quite easily from web tension was studied by Vedrines et al. [6]. In addition to this, sliding FFT was used to separate force (process and machine created) and free vibrations. In Transient effect of moving head and tap is analyzed by Sundaram et al. [26], where analytical model for web deflection is proposed and effect of tension, stiffness, speed, damping and edge is investigated. A camera and laser dots have been used to measure web position with respect to the camera by Doignon et al. [27]. Due to the variation of web position, frequencies were determined in an economical way. The source of variations can be roller eccentricity, tension variation, motor torque, temperature variation and web sliding. Naiver stoke simulations were used to determine flutter amplitude and air flow around the web by Watanabe et al. [27]. Potential flow analysis was used for parametric study and viscous flow analysis was used for web fluttering, is time domain base while potential flow is based on frequency domain analysis. The complexity of web motion is due to variations in tension, speed, geometric and material properties and airflow around the web studied by Watanabe et al. [28]. Experimentally all these effects are found to be important for web flutter. Visualization test is used for the flutter mode and air-flow around the web. Dguyen has used contact-less sensors (Infrared optical sensor) to measure web fluttering which can give fluttering amplitude and

frequency [29]. As frequency is proportional to web tension hence, it was measured and control was applied to maintain the required level of tension for stable web operation. A detailed method was given to control web tension variations by Wells [30]. A contact-less sensor is used to measure web flutter, its amplitude and determine web tension. Based on this, a control strategy is applied to have proper tension in the web. High amplitude vibrations limit the detector range and light source is sensitive to fiber dust and ambient light as well. Reciprocating motion of the web is analyzed by R.Ahola [31], where a light source and its detector was used for directing light on the web and reflected light was received by detector which was susceptible to both machine vibrations and dust contamination. Stanley et al. [34] has used an array of contact-less proximity sensor was used for measuring sheet flatness. Tension is applied to sheet for removing compressive strains and an average of two measurements is taken for analyzing transverse vibration of sheet by its reciprocating operation. A novel collimated laser sensor was used by Seshadri et al. [32], where the fiber array receives the reflected light from the web, in such a way that its direction is parallel to the web flutter. Furthermore, this sensor is direct, linear and unaffected by web properties. Simple and no complex signal conditioning is required. After installation, no need of recalibration. Due to the use of optical fiber, signal processing is done far away from measurement area, hence it can be used in intense hot and humid environment, but still no temperature stability control. Y. Chang et al. [33], investigated critical flow speed, wave speed, wavelength and flutter frequency by using potential flow theory. Experiments were carried with the wind tunnel test, where tension and flow directions are perpendicular to each other. Instruments such as stroboscope and vibro-meter were used for measurement web vibrations. Nguyen et al. [35] has used air pressure in web fluttering to generate a analogue signal and then processed to measure web flutter.

All the sensors discussed have pros and cons in their own capacity. For example,

a complex computational method is proposed which could be affected by low quality images of the camera [27]. An infrared proximity sensor was used to measure web flutter but it cannot be used in sunlight and accuracy of range can be affected [29]. The light reflects from web surface at specific reflection angles, which makes it sensitive to angle of reflection and amplitude of vibration could be affected [30]. Here the web vibrations mainly depend upon time travel of light beam from source to receiver and susceptible to both machine vibrations and dust contamination [31]. The position of fiber array and source may be critical and a small deviation in angle can affect the received light intensity [32]. Stroboscope and laser vibro-meter were used for web vibration measurements and such instruments required complicated and expensive signal conditioning [33]. Web vibrations were determined from variations in pressure signal generated by pressure sensor which are susceptible to jet exposure and air drying environment [35]. Literature review revealed that each sensor with a sensing technique has some limitations such as:

- Problems related to light intensity of experiential environment.
- Frequent calibration.
- Web material reflectance variations may create problems in performance.
- Dust contamination and extreme surrounding conditions have strong effect on sensor's performance.
- Exposure to air jet and air dryer could cause changes in pressure signal.

Further, these sensors need frequent calibration as none of them provide direct measurement of web flutter. The utilized sensor for measuring web transverse vibration is found promising in dealing with existing limitations associated with the sensors as reported in the literature. Advantages of this new utilized displacement sensor in this study are:

- It is simple and can be operated easily as a USB plug-in device.
- The displacement sensor needs no complex signal conditioning.
- It has two factory calibrations, one mirror and another diffuse surface. It can be easily calibrated for other material surfaces and could store up to 25 calibrations data.
- It measure the web displacement up to 0.180 μm which can be considered as true displacement.
- It has its temperature control ability and reaches easily to thermal equilibrium for operation.
- It can be used to measure both transverse and longitudinal displacements depend upon its orientation with respect to the target surface.
- Due to its compact size and light weight, it can be place at various positions on the web handling platform.

CHAPTER 3

POLYETHYLENE TEREPHTHALATE (PET) WEB VISCOELASTIC PROPERTIES

The mechanical properties of PET in stretching are highly dependent on temperature, strain, strain rate reported [36]. It has many applications in fiber, food industry for making clothes and manufacturing containers for liquids. It can be found with fiber glass for resin applications in engineering. Its importance is due to its use as a web in printing industry, cheap availability, good chemical and mechanical properties and variety of metals such as gold, aluminum, copper etc can be printed on it. The viscoelastic behavior of PET could affect the dynamic response and transverse vibration during axial motion. Therefore, characterized for viscoelastic properties at room temperature using Instron 5869 machine. This PET is also called Mylar, a commercial name and a product made from resin PET.

3.1 Introduction to Instron 5869 material testing machine

The Instron 5869 testing machine can be used for determining creep and relaxation properties of Mylar PET. The Instron machine has a control software (bluehill) which has multiple templates for different applications and one of the template is for creep analysis. Mylar PET is used in all experiments with the same setup at room temperature as shown in Figure 3.1.

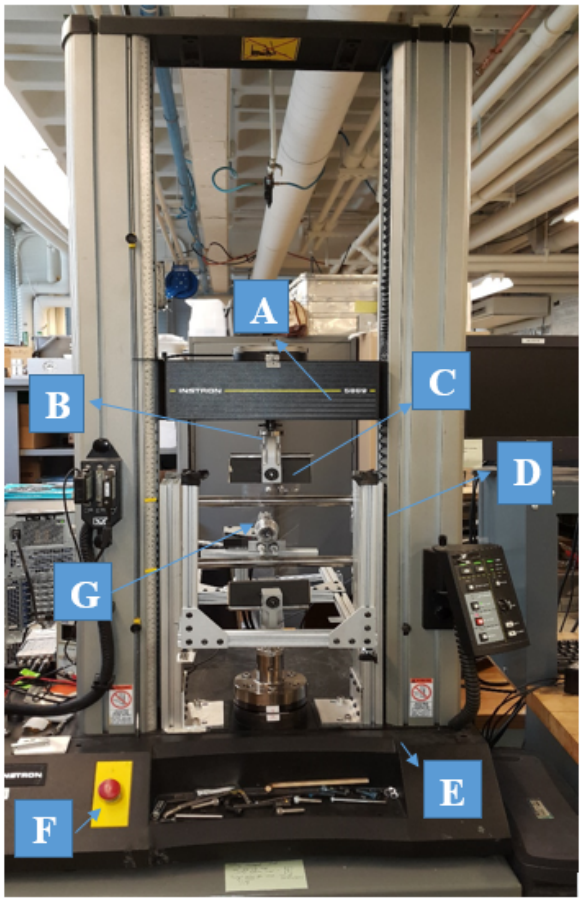

Figure 3.1: Labeled picture of the Instron 5869 load frame.

- (A) Cross-head: The part of the load frame that moves up during a tensile test or down during a compression test.

- (B) Load cell: Measure the applied load and is designed for $\pm$ 1 kN maximum load.
- (C) Sample grips: The sample grips hold sample during test, come in many shapes and sizes from threaded to clamp.
- (D) Upper and lower cross-head limits: Trip switches for maximum height allowing cross-head to travel during a test.
- (E) Manual up/down toggle: Moves cross-head up and down manually following user command. The toggle only works however when software is loaded on computer and using this button without software being loaded may result in machine locking.
- (F) Emergency stop: Safety toggle pressing will immediately shut down all machine operations to avoid any unpleasant situation.
- (G) Sample: It is gripped between two jaws shown in Figure 3.1.

The physical and geometric parameters for Mylar PET used experiments are shown in Table 3.1.

Table 3.1: Mylar physical properties

Parameters	**Definitions**
Web span length	11 in
Web width	4.5 in
Web thickness	3 mil
PET dynamic viscosity	2393.123 ksi s [36,37]
PET density	0.05022 Ibm/in^3
Elastic modulus	725188 psi
Web tension	25 Ibf
Web stretching speed	0.1,0.2,0.3,0.4,0.5 in/min
Hold duration	3.98 or 4 min
End of test time	5 min
PET melting temperature	254 $\mathring{C}$
Experiment temperature	24 $\mathring{C}$

3.2 Experimental work of PET characterization

In this section viscoelastic properties (creep and relaxation) of Mylar PET are experimentally investigated at room temperature.

3.2.1 Creep analysis of Mylar PET

Creep can be defined as a time dependent permanent deformation under the application of constant mechanical stresses. It occurs due to high stresses which are less than the yield strength of the material under consideration. Creep is more severe at high temperature and increases with high temperature of the material and environ-

ment. Viscoelastic materials have both properties of viscosity and elasticity which can be modeled by using a spring and dash-pot in many combinations such as Maxwell and Voight models etc. Viscoelastic materials don't follow Hook's law and shows nonlinearity, therefore relaxation and creep are used to define this behavior.

Mylar PET is usually resistant to creep and tests are performed at room temperature for different web stretching speeds. For the first experiment 0.1 in/min stretching speed is used. Figure 3.2a shows that a constant load of 25 Ibf is applied to PET web and reached to 25 Ibf within 22 sec, then maintained for 4 min and finally strain produced is increased. In Figure 3.2b, an increase in strain after constant load application is shown for clear visualization. This increase in strain is from 0.290 % to 0.297 % with high fluctuations due to web slippage which clearly indicates viscoelastic behavior and this means the sample deformation is time dependent.

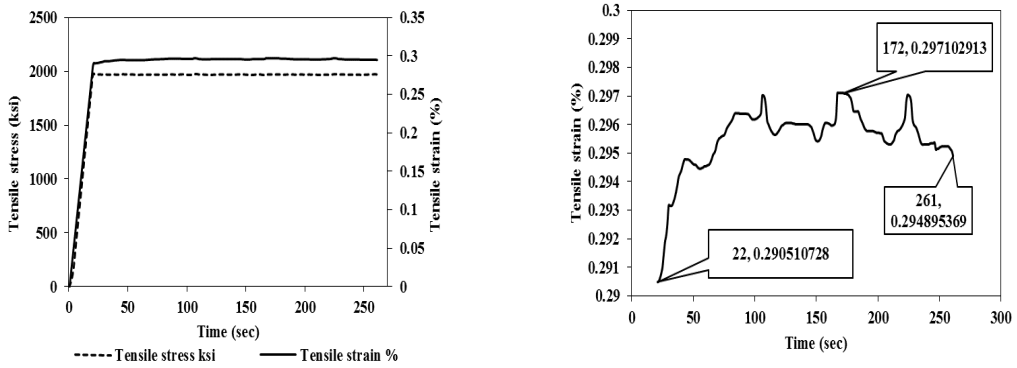

(a) Strain rate at 0.1 (in/sec) (b) Strain (%) increase

Figure 3.2: Creep results from experiment no.1.

The main difference with this experiment no.2 as compared to the experiment no.1 is that, now the specimen is stretched quickly with a stretching speed of 0.2 in/min and it reached to 400 oz or 25 Ibf within 11 sec instead of 22 sec as compared to the experiment no.1. Similar to the experiment no.1, load is held constant for 4 min duration to observe strain variation with time. During constant holding force of 400 oz or tensile stress of 1980 ksi, similar strain behavior of an increase in magnitude

is observed. During constant loading and 4 min interval, an increase from 0.311 % to 0.314 % is observed in the strain and then it started fluctuating. In Figure 3.3a and Figure 3.3b experimental results are presented. In Figure 3.3b after 11 seconds, there is a sudden decrease in strain % and this is because of the web slippage during the experiment.

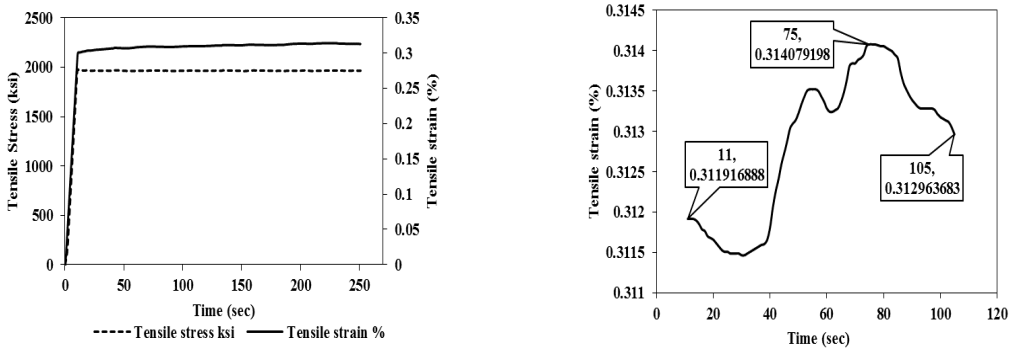

(a) Strain rate at 0.2 (in/sec) (b) Strain (%) increase

Figure 3.3: Creep results from experiment no.2.

Now the stretching speed of the web is increased to 0.3 in/min in experiment no.3 with a reaching time of 8 sec to 25 Ibf load. Due to the constant stress, strain increased after maintaining the load for a specific interval of 4 min. Now strain is increased from 0.302 % to 0.313 % due to its viscoelastic behavior and fluctuations due to slippage are less as compared to the experiment no.1 and experiment no.2 as shown in Figure 3.4a and Figure 3.4b.

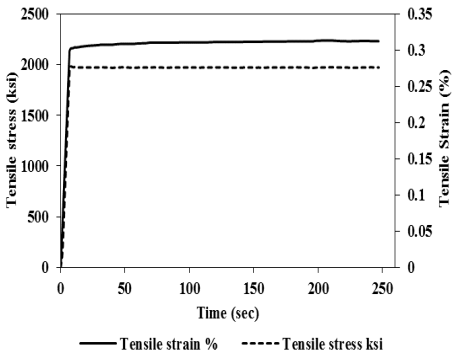

(a) Strain rate at 0.3 (in/sec)

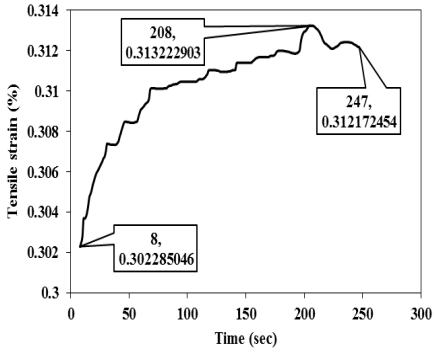

(b) Strain (%) increase

Figure 3.4: Creep results from experiment no.3.

In experiment no.4 web stretching speed is raised to 0.4 in/min and it reached in 6 sec to final load of 25 Ibf. By increasing the speed, PET material reached to its final load in 6 sec and then held constant for 4 min duration. As the viscoelastic behavior is time dependent and fast stretching speed absorb less force, due to which strain increased from 0.294 % to 0.305 %, which is less when compared to experiment no.3 in Figure 3.5a and Figure 3.5b.

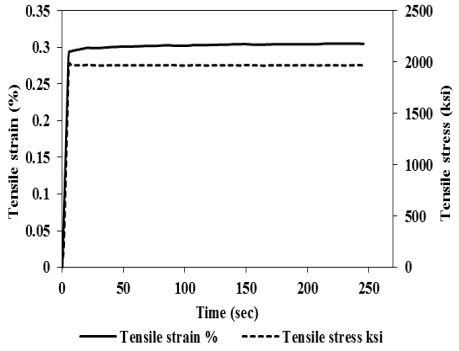

(a) Strain rate at 0.4 (in/sec)

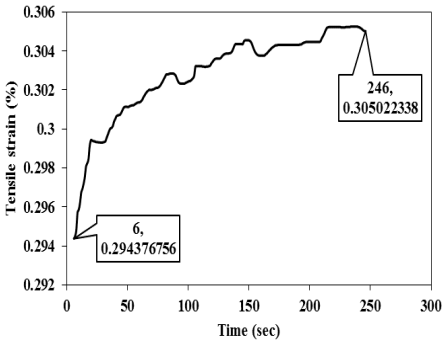

(b) Strain (%) increase

Figure 3.5: Creep results from experiment no.4.

From all of the four experiments it might be concluded that creep occurred in Mylar PET at room temperature. When the web is stretched and then held constant for a specific duration, strain increases, which confirms the existence of creep. It is observed that when stretching speed increases from 0.1 in/min to 0.4 in/min, the percent

increase in strain decreases because the PET sample absorbs less force. In addition to this, it is observed that from low to high web stretching speed the fluctuations of strain decreases and the reason for these fluctuations was found to be the slippage of web during stretching. It is recommended to clearly analyze these properties, the experiment time should be increased to relax sample material properly. Mathematically, creep behavior can be investigated using different viscoelastic models, such as Kelvin Voight model which says that, when a sudden stress is applied, deformation approaches for pure elastic material and decaying exponentially:

$$\epsilon(t) = \frac{\sigma_0}{E}\left(1 - e^{\left(-\frac{Et}{\eta}\right)}\right), \tag{3.1}$$

where, $\epsilon(t)$ represents time dependent strain, t is time, σ_0 is constant stress and E is modulus of elasticity.

3.2.2 Relaxation analysis of Mylar PET

Stress relaxation can be defined as the decrease in stress observed for the same amount of strain generated in the structure. This relaxation depends upon time span length, temperature and stress level of specimen. The same experimental setup is used for both creep and relaxation analysis.

In relaxation experiment no.1, first an extension is defined, such as 98.5 mil in computer software and then experiment is started to obtain this extension by stretching web specimen. The cross-head reached to 98.5 mil extension within 37 sec, with a stretching speed of 0.1 in/min. The web specimen is held constant at 98.5 mil for a duration of 4 min and stress behavior with time is observed. Relaxation plot is obtained and stress relaxed from 3038 ksi to 2927 ksi in 4 min as shown in Figure 3.6a and Figure 3.6b.

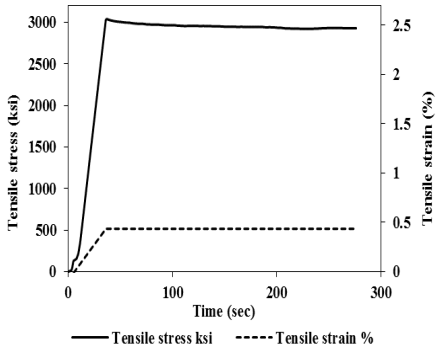

(a) Stress rate at 0.1 (in/sec)

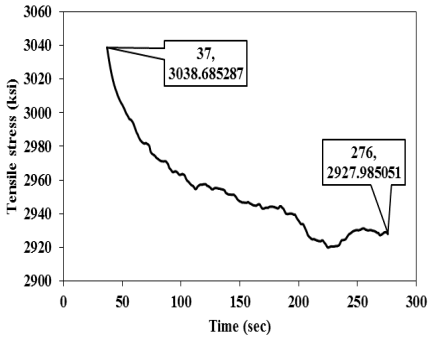

(b) Stress (ksi) decline

Figure 3.6: Relaxation results from experiment no.1.

In experiment no.2, web stretching speed of 0.2 in/min is used and it took 17 sec to reach 98.5 mil web extension. Stress relaxed from 3015 ksi to 2901 ksi during 4 min time and reaching to the required extension within 17 sec as shown in Figure 3.7a and Figure 3.7b.

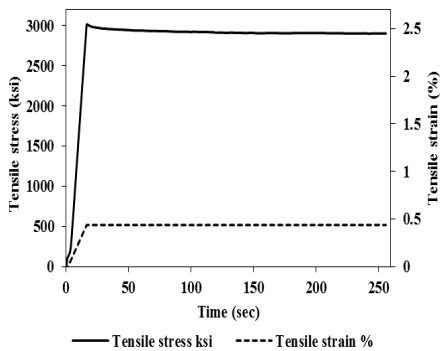

(a) Stress rate at 0.2 (in/sec)

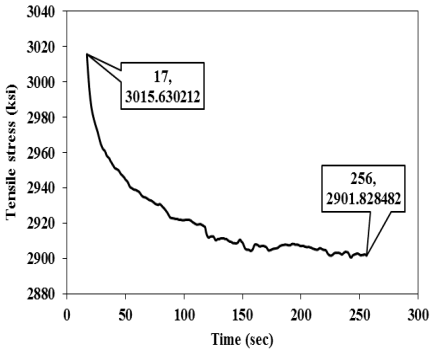

(b) Stress (ksi) decline

Figure 3.7: Relaxation results from experiment no.2.

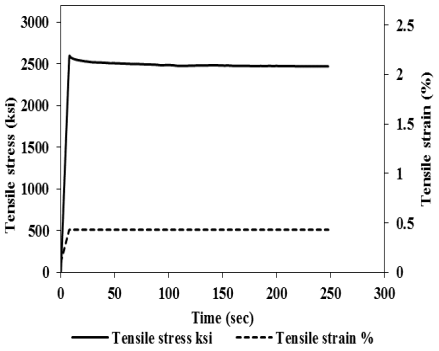

(a) Stress rate at 0.3 (in/sec)

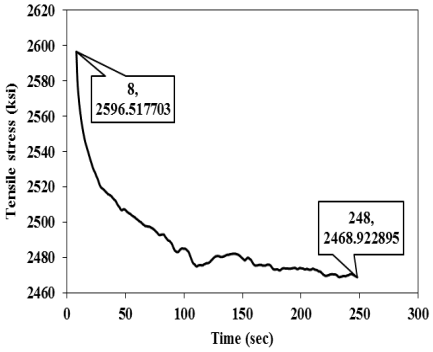

(b) Stress (ksi) decline

Figure 3.8: Relaxation results from experiment no.3.

In experiment no.3, web stretching speed of 0.3 in/min is used and it took 8 sec to reach 98.5 mil extension. The cause of relaxation is the molecular movement in material structure. Stress relaxed from 2596 ksi to 2468 ksi during the 4 min time shown in Figure 3.8a and Figure 3.8b.

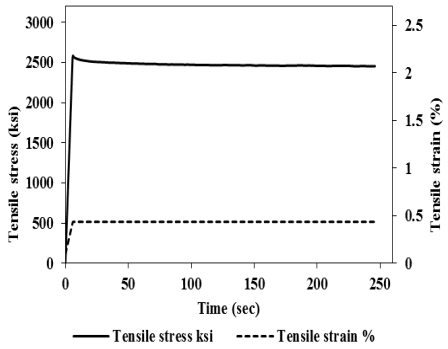

(a) Stress rate at 0.4 (in/sec)

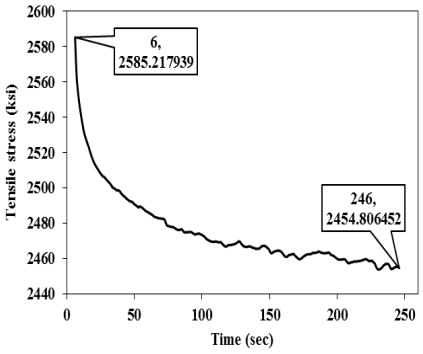

(b) Stress (ksi) decline

Figure 3.9: Relaxation results from experiment no.4.

In the final experiment no.4, web stretching speed of 0.4 in/min is used and it took 6 sec to the sample, to reach 98.5 mil extension. Stress relaxes from 2585 ksi to 2454 ksi during the 4 min time shown in Figure 3.9a and Figure 3.9b.

It can be concluded from all four experiments that stress relaxation of PET web occurs at room temperature, thus confirming its viscoelastic behavior. Mathematically, relaxation behavior can be investigated using different viscoelastic models such

as Kelvin Voight model where we would free the material at time t_1, then the elastic element would retard the material back until the deformation becomes zero:

$$\epsilon(t > t_1) = \epsilon(t_1)\left(1 - e^{-\frac{E}{\eta}(t-t_1)}\right), \tag{3.2}$$

where, $\epsilon(t_1)$ represents time dependent strain, t is time, σ_0 is constant stress and E is modulus of elasticity.

3.2.3 Force-displacement and stress-strain analysis of Mylar PET

The first experiment was performed to get force-displacement relationship of Mylar PET. From experimental data following plots are obtained which show a linear relationship between force and displacement for a 20 Ibf load as shown in Figure 3.10a.

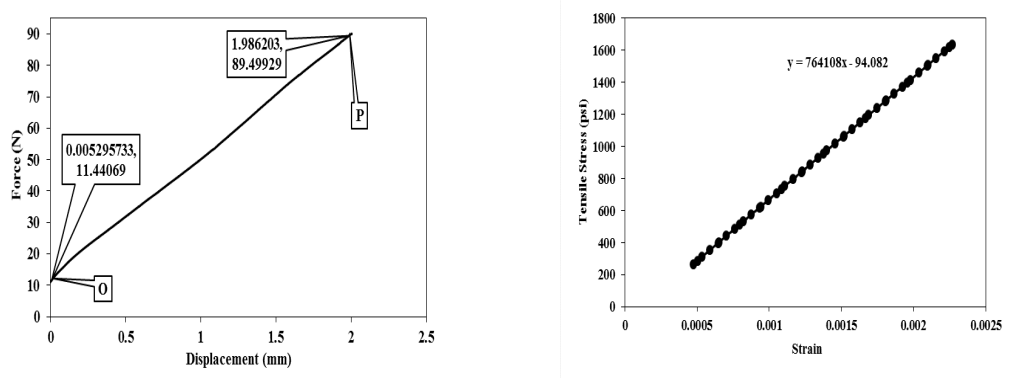

(a) Force-displacement relationship for PET (b) Stress-strain relationship for PET

Figure 3.10: Tensile properties

Typical stress-strain relationship can be seen in Figure 3.10b. When stress increased within the elastic limit at room temperature strain increased as well. In this experiment only proportional and elastic limit were used where load is released before the elastic limit, specimen went back to its original position and follows Hook's law. This Hook's law from the plot can be defined between points O and P. As OP is a

straight line which shows that Hook's law of force-displacement is followed up to the point P. From stress-strain relationship modulus of elasticity can be determined and slope of the line in region where stress is proportional to strain called modulus of elasticity. In Figure 3.10b, the slope is 764108 psi which can be verified from data sheet [38].

CHAPTER 4

ANALYTICAL INVESTIGATION OF TRANSVERSE VIBRATION OF AXIALLY MOVING PET WEB

In this chapter analytical models of elastic and viscoelastic axially moving string are presented. For the elastic case, the equation of motion is linearized and the dynamics of amplitude time history response are obtained. Kelvin-Voight model is used to formulate the viscoelastic string and amplitude time history response is compared to that of elastic moving string. In the last portion of the chapter Comsol simulations of stationary string and thin plate models are used to validate web frequency results from analytical solutions.

4.1 Problem formulation of axially moving elastic string

Formulation of the string is based on an axially moving string with a constant axial speed v and constant web tension force P is applied along the x-axis of string. String is considered to be uniform along the web length with a cross sectional area of A, modulus of elasticity E and density (mass per unit length) ρ. Figure 4.1 shows a

schematic for the vibrating running web.

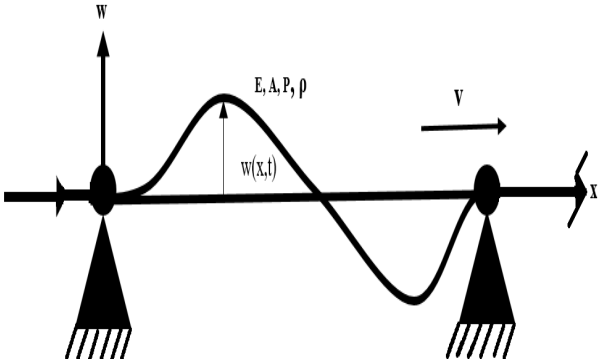

Figure 4.1: Simply supported axially moving string exaggerated vibration.

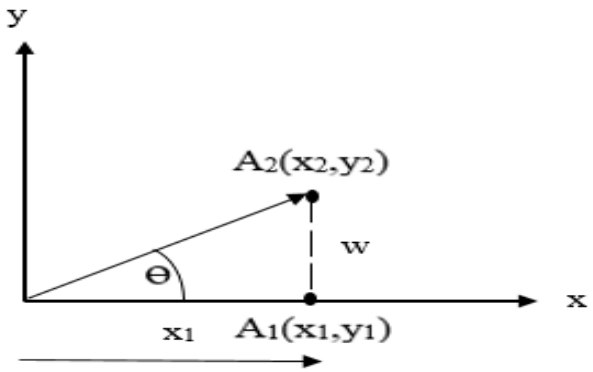

Figure 4.2: Deformed segment of the moving string.

Let assume that A_1 be the initial position of a point on the string at distance x in axial direction with its coordinates (x_1, y_1), as illustrated in Figure 4.2. The final position of point A_1 after deformation is A_2 with coordinates (x_2, y_2). The point is displaced at a distance w in the transverse direction. The new coordinates of point A_2 are:

$$x_2 = x_1 \quad and \quad y_2 = y_1 + w,$$

as $y_1 = 0$ and dropping the subscript from both x_1 and y_1,

$$x_2 = x \quad and \quad y_2 = w. \tag{4.1}$$

Differentiating Equation (4.1) with respect to x yields,

$$dx_2 = dx \quad and \quad dy_2 = \left(\frac{dw}{dx}\right) dx. \tag{4.2}$$

Therefore, length of the deformed configuration can be expressed as follows,

$$ds = \sqrt{(dx_2)^2 + (dy_2)^2},$$

$$ds = \sqrt{1 + (w_{,x})^2}\, dx. \tag{4.3}$$

Where the subscript notation denotes partial differentiation with respect to x. The elongation of differential element is,

$$ds - dx = \left(\sqrt{1 + (w_{,x})^2} - 1\right) dx. \tag{4.4}$$

From elongation of the deformed element in Equation (4.4), strain can be determined as,

$$\epsilon = \frac{ds - dx}{dx} = \left(\sqrt{1 + (w_{,x})^2} - 1\right) = -1 + (1 + (w_{,x})^2)^{\frac{1}{2}}. \tag{4.5}$$

Using binomial series expansion on Equation (4.5) given below,

$$(1 + nx)^n = 1 + \frac{nx}{1!} + \frac{n(n-1)x^2}{2!} + ... \tag{4.6}$$

Applying Equation (4.6) to Equation (4.5) as follows,

$$\epsilon = -1 + \{1 + \left(\frac{1}{2}\right)(w_{,x})^2 + \frac{\left(\frac{1}{2}\right)\left(1 - \frac{1}{2}\right)((w_{,x})^2)^2}{2!} + ...\}. \tag{4.7}$$

Neglecting 4^{th} and higher order terms in Equation (4.7), yields simplified equation

(4.8) representing a geometric nonlinearity reported in [39].

$$\epsilon = \frac{1}{2} w_{,x}^{2} \,. \tag{4.8}$$

Kinetic energy of the string:

String moves along the x-axis has Kinetic Energy (K.E). The longitudinal and transverse speed components can be derived by differentiating Equation (4.2) with respect to time t,

$$\frac{dx_2}{dt} = \frac{dx}{dt} = v. \tag{4.9}$$

Where v is the longitudinal velocity component. By applying product rule to find the transverse speed components, i.e.

$$\frac{dy_2}{dt} = \left(\frac{dw}{dx}\right)\frac{dx}{dt} + \left(\frac{d^2w}{dt}\right)dx. \tag{4.10}$$

Equation (4.10) represents the transverse speed component that is equal to $w_{,t} + vw_{,x}$, where, x and t notations show partial differentiation with respect to x and t. Thus, kinetic energy of the axially moving string is $T = \frac{1}{2}mv^2$ which results in,

$$K.E = \frac{1}{2}\rho A \int_0^L v^2 + (w_{,t} + vw_{,x})^2, \tag{4.11}$$

where, $\rho A = \frac{m}{l}$ is mass per unit length.

Potential energy of the string:

Potential Energy (P.E) is due to tension in the web and its axial deformation is given by,

$$P.E = \int_0^L \left(P\epsilon + \frac{1}{2}EA\epsilon^2\right)dx. \tag{4.12}$$

Where, ϵ from Equation (4.8) represents nonlinear strain and axial stress σ can also

be represented as follows,

$$\epsilon = \frac{1}{2} w_{,x}^{2} \qquad and \qquad \sigma = E\epsilon.$$

Virtual work due to non-conservative force:

The variation of non-conservative force is given by considering viscous damping coefficient μ times transverse speed $w_{,t}$ as follows,

$$V.W = \int_{t_1}^{t_2} \delta W dt = \int_{t_1}^{t_2} (-\mu w_{,t}) \delta w dt. \tag{4.13}$$

Hamilton's Principal:

The Hamilton's principal to obtain equation of motion is,

$$\delta I = \int_{t_1}^{t_2} (\delta K.E - \delta P.E + \delta V.W) dt. \tag{4.14}$$

Substituting K.E, P.E and V.W in Equation (4.14) yields,

$$\delta \int_{t_1}^{t_2} \left(\frac{\rho A}{2} \int_0^L \left[v^2 + (w_{,t} + v w_{,x})^2 \right] dx \right) dt$$

$$-\delta \int_{t_1}^{t_2} \left(\int_0^L \left[\frac{P}{2} w_{,x}^{2} + \frac{EA}{8} w_{,x}^{4} \right] dx - \mu w_{,t}\, \delta w \right) dt = 0.$$

Expanding the above equation and multiplying by 2 as follows,

$$\delta \int_{t_1}^{t_2} \left(\left(\rho A \int_0^L \left[v^2 + (w_{,t}^{2} + v^2 w_{,x}^{2} + 2v w_{,t}\, w_{,x}) \right] dx \right) \right.$$

$$\left. - \left(\int_0^L \left[P w_{,x}^{2} + \frac{EA}{4} w_{,x}^{4} \right] dx - 2\mu w_{,t}\, \delta w \right) dt \right) = 0. \tag{4.15}$$

For detailed derivations of each term of Equation (4.15) please refer to appendix A. Variation of non-conservative forces is given by viscous damping coefficient μ times

transverse speed $w_{,t}$ as follows,

$$\int_{t_1}^{t_2} \delta W dt = \int_{t_1}^{t_2} -\mu w_{,t}\, \delta w dt. \tag{4.16}$$

Equation of motion is obtained by variation in kinetic and potential energies plus work done by non-conservative force, therefore integrating all the terms over time yields,

$$\int_{t_1}^{t_2} \delta \mathcal{L} dt = \int_{t_1}^{t_2} (\delta K.E - \delta P.E + \delta V.W) dt = 0. \tag{4.17}$$

$$\int_{t_1}^{t_2} \delta \mathcal{L} dt = \rho A \int_{t_1}^{t_2} v^2 x\Big|_{x=0}^{x=L} dt - \rho A \int_{t_1}^{t_2}\int_0^L w_{,tt}\, \delta w dx dt + \rho A v^2 \int_{t_1}^{t_2} w_{,x}\, \delta w\Big|_{x=0}^{x=L} dt$$

$$-\rho A v^2 \int_{t_1}^{t_2}\int_0^L w_{,xx}\, \delta w dx dt + 2v\rho A \int_{t_1}^{t_2} w_{,t}\, \delta w\Big|_{x=0}^{x=L} dt - 2\rho A v \int_{t_1}^{t_2}\int_0^L w_{,xt}\, \delta w dx dt$$

$$-P \int_{t_1}^{t_2} w_{,x}\, \delta w\Big|_{x=0}^{x=L} dt + P \int_{t_1}^{t_2}\int_0^L w_{,xx}\, \delta w dx dt - \frac{1}{4} EA \int_{t_1}^{t_2} w_{,x}^2\, w_{,x}\, \delta w\Big|_{x=0}^{x=L} dt$$
$$+\frac{1}{4} EA \left(\int_{t_1}^{t_2}\int_0^L w_{,x}^2\, w_{,x} \right)_x \delta w dx dt - 2\int_{t_1}^{t_2} \mu w_{,t}\, \delta w dt = 0.$$

Above equation must hold for any arbitrary δw and $w_{,x}$. The integrand should be zero which gives equation of motion governing the transverse vibration of axially moving string. Now gathering terms with coefficients of δw yields,

$$\int_{t_1}^{t_2} \delta \mathcal{L} dt = -\rho A \int_{t_1}^{t_2}\int_0^L w_{,tt}\, \delta w dx dt - \rho A v^2 \int_{t_1}^{t_2}\int_0^L w_{,xx}\, \delta w dx dt$$

$$-2\rho A v \int_{t_1}^{t_2}\int_0^L w_{,xt}\, \delta w dx dt + P \int_{t_1}^{t_2}\int_0^L w_{,xx}\, \delta w dx dt$$

$$+\frac{1}{4} EA \left(\int_{t_1}^{t_2}\int_0^L w_{,x}^2\, w_{,x} \right)_x \delta w dx dt - 2\int_{t_1}^{t_2} \mu w_{,t}\, \delta w dt = 0.$$

Simplifying and multiplying by negative sign gives,

$$\rho A w_{,tt} + \rho A v^2 w_{,xx} + 2\rho A v w_{,xt} - P w_{,xx} - \frac{1}{4} EA \left(w_{,x}^2 \, w_{,x} \right)_x + 2\mu w_{,t} = 0.$$

Where, $\rho A = \rho_l$ and giving the following simplified equation,

$$w_{,tt} + 2v w_{,xt} - \left(\frac{P}{\rho_l} - v^2 \right) w_{,xx} - \frac{3EA}{4\rho_l} w_{,x}^2 \, w_{,xx} + \frac{2\mu}{\rho_l} w_{,t} = 0. \tag{4.18}$$

Finally Equation (4.18) is obtained which is a second order nonlinear partial differential equation of a moving string in space and time. Therefore, its solution requires two boundary and initial conditions which are:

$$w(0,t) = 0, \quad w(L,t) = 0, \quad and \quad w(x,0) = 0, \quad w_{,t}(0,t) = 0. \tag{4.19}$$

4.1.1 One term Galerkin discretization of governing equation of axially moving elastic string

Galerkin method is used for discretization, therefore let us assume that,

$$w(x,t) = T_n \sin\left(\frac{n\pi x}{L} \right).$$

Where, $\sin(\frac{n\pi x}{L})$ is the first mode shape of vibration for the simply supported stationary string and T_n is called generalized displacement reported in [40]. For one term approximation n = 1,

$$w(x,t) = T \sin\left(\frac{\pi x}{L} \right). \tag{4.20}$$

Substituting Equation (4.20) into Equation (4.18) yields,

$$\sin\left(\frac{\pi x}{L}\right)\ddot{T}+\frac{2v\pi}{L}\cos\left(\frac{\pi x}{L}\right)\dot{T}+\frac{\pi^2}{L^2}\left(\frac{P}{\rho_l}-v^2\right)\frac{\pi^2}{L^2}\sin\left(\frac{\pi x}{L}\right)T$$
$$+\frac{3}{4}\frac{EA}{\rho_l}\left(\frac{T\pi}{L}\cos\left(\frac{\pi x}{L}\right)\right)^2\frac{\pi^2}{L^2}\sin\left(\frac{\pi x}{L}\right)T+\frac{2\mu}{\rho_l}\sin\left(\frac{\pi x}{L}\right)\dot{T}=0.$$

Multiplying this equation by the first mode shape of vibration and integrating from 0 to L yields,

$$\ddot{T}+\frac{2\mu}{\rho_l}\dot{T}+\frac{\pi^2}{L^2}\left(\frac{P}{\rho_l}+v^2\right)T+\frac{3EA\pi^4}{16\rho_l L^4}T^3=0. \tag{4.21}$$

Substituting Equation (4.21) into Equation (4.20), gives amplitude time history response.

To study the amplitude time history response of an axially moving string, air damping is of vital importance, because of its dependency upon magnitude of surrounding air pressure. For instance, if for a space vehicle, the vibration test is conducted under ambient pressure conditions, the effect of air damping on the system response will be different than the same test performed in reduced pressure environment. Thus, for a complete investigation of such systems, air damping must be included. The level of air damping is highly dependent upon conditions of pressure environment therefore, up to value of 0.001 ($5.71*10^{-6}$) N.s/m (Ibf.s/in) air damping is used in [41] and free transverse vibration decay with air damping of a thin vibrating beam [42]. From Equation (4.20), results show that air damping has a strong effect on the amplitude time history response, because its amplitude decreased with the increase of air damping shown in Figure 4.3.

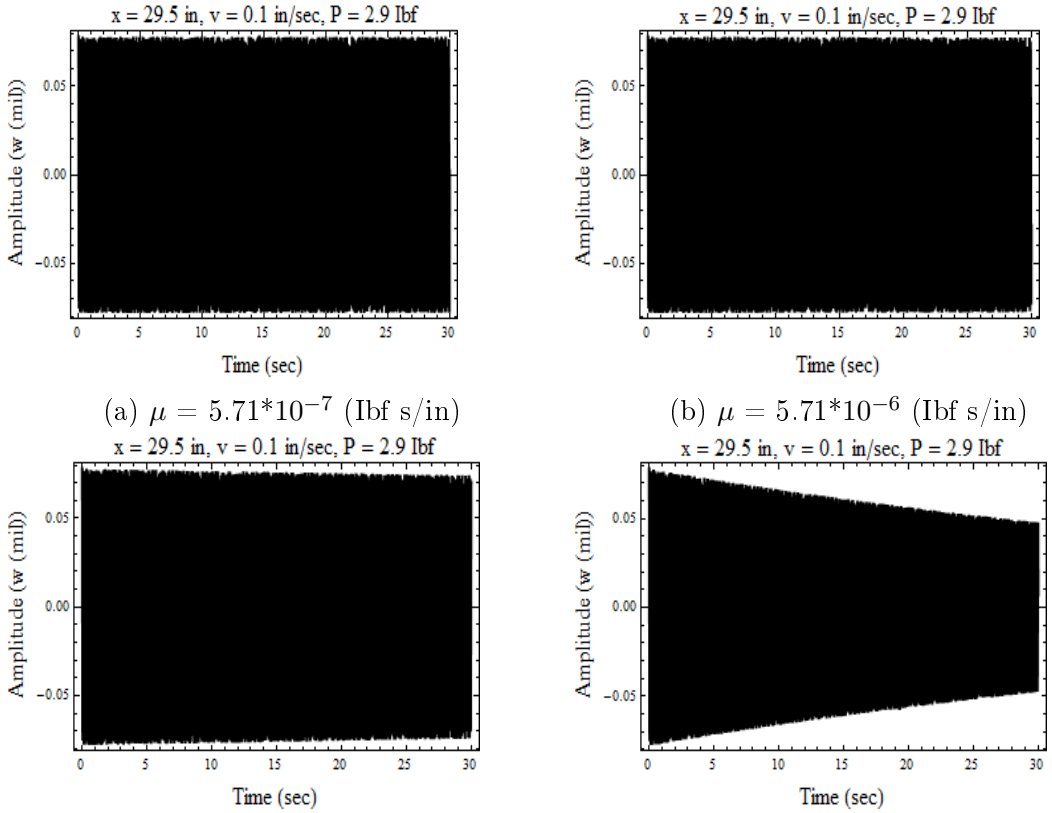

(a) $\mu = 5.71{*}10^{-7}$ (lbf s/in)

(b) $\mu = 5.71{*}10^{-6}$ (lbf s/in)

(c) $\mu = 5.71{*}10^{-5}$ (lbf s/in)

(d) $\mu = 5.71{*}10^{-4}$ (lbf s/in)

Figure 4.3: Effect of air damping coefficient on amplitude time history response of elastic string.

Effect of axial web speed on amplitude time history response of a moving elastic web is also analyzed. It is concluded from Figure 4.4 that axial web speed has no significant effect on amplitude time history response and this negligible effect can be confirmed from [25].

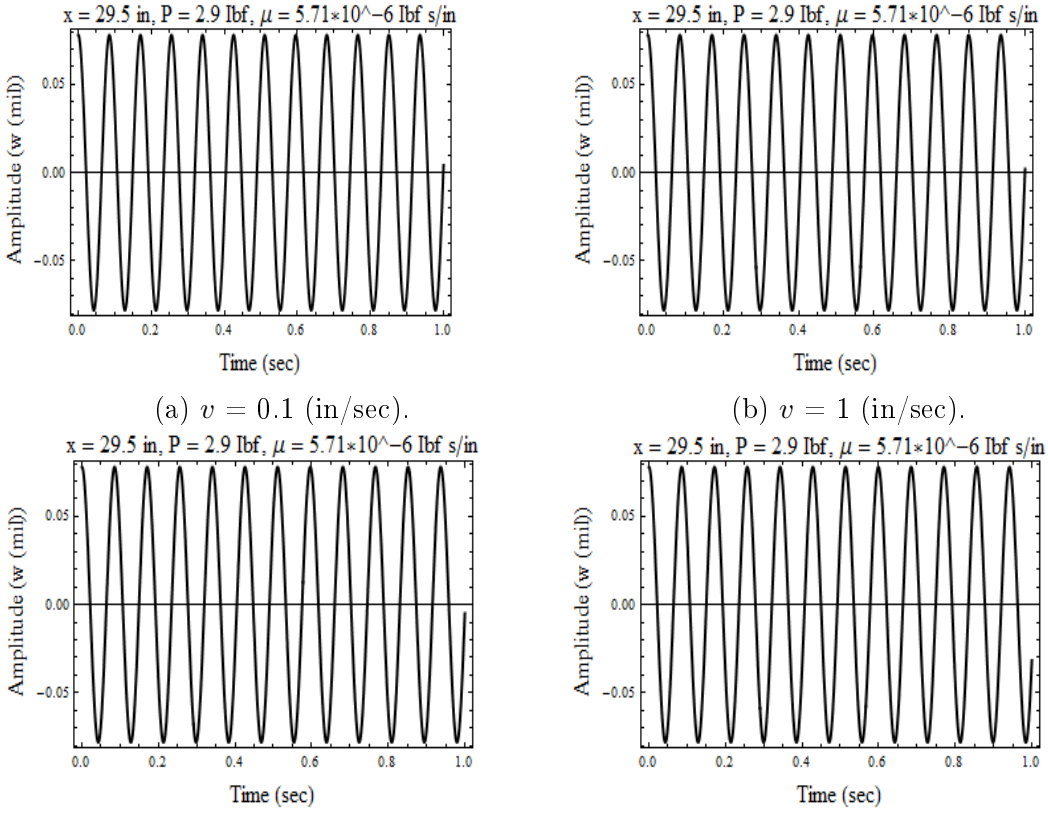

(a) $v = 0.1$ (in/sec). (b) $v = 1$ (in/sec).

(c) $v = 2$ (in/sec). (d) $v = 4$ (in/sec).

Figure 4.4: Effect of web velocity on amplitude time history response of elastic string.

Effect of web tension on amplitude time history response of moving elastic web is also analyzed. It shows, that web tension has significant effect on the period of amplitude time history response. With the increase of web tension, period of amplitude time history response decreased which can be clearly seen in Figure 4.5.

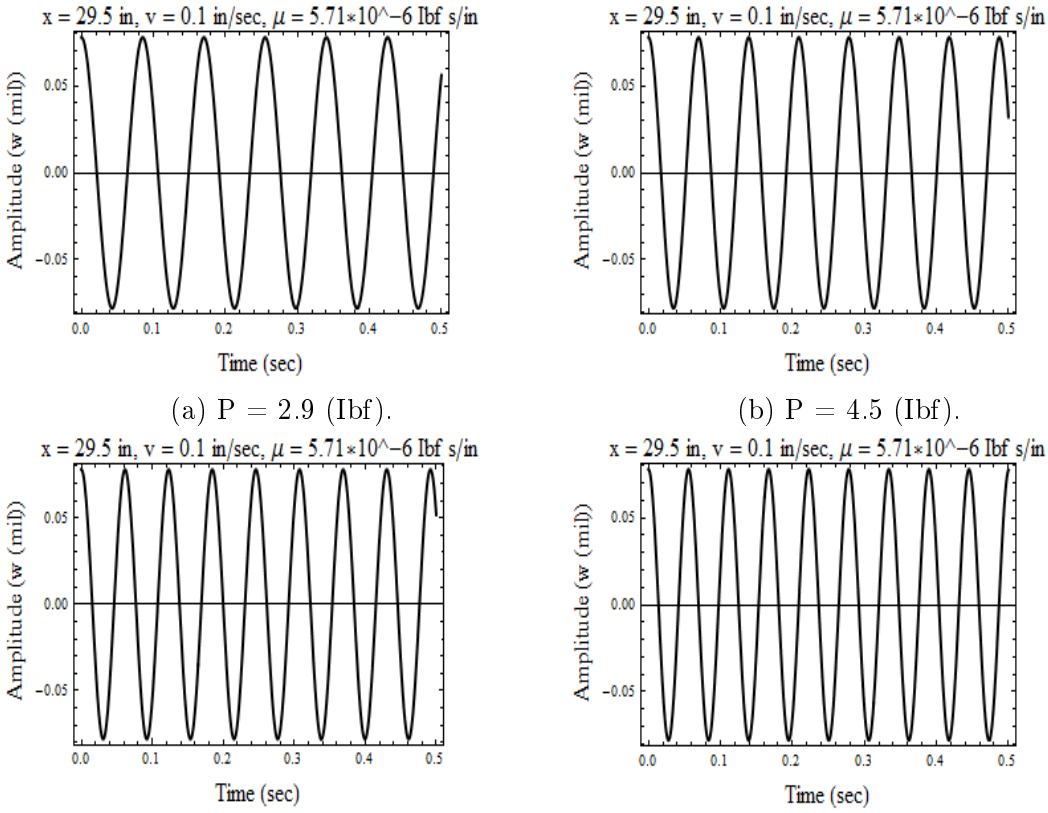

(a) P = 2.9 (lbf). (b) P = 4.5 (lbf).

(c) P = 5.8 (lbf). (d) P = 7.1 (lbf).

Figure 4.5: Effect of web tension on amplitude time history response of elastic string.

4.2 Problem formulation of axially moving viscoelastic string

PET web behaves as a viscoelastic material in stretching and important to consider its viscoelasticity in the dynamic modeling of a roll-to-roll system. A viscoelastic string with density of ρ, cross-sectional area of A, travels with a constant axial speed

v and simply supported at both ends. Kelvin-Voight viscoelastic model is selected to describe viscoelastic properties of PET web. String obeys Kelvin-Voight model [43,44] and is composed of a linear spring and a linear dash-pot are connected in parallel as shown in Figure 4.6. The corresponding linear differential operator $\hat{E}$ for Kelvin-

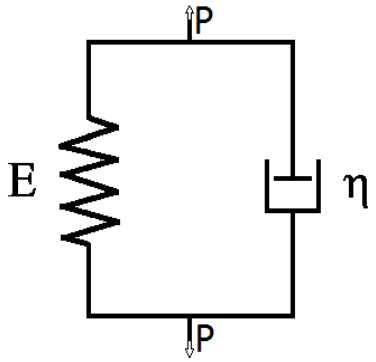

Figure 4.6: Kelvin-Voight viscoelastic model.

Voight viscoelastic model is,

$$\hat{E} = E + \eta \frac{\partial}{\partial t}. \tag{4.22}$$

Where, E is elastic stiffness constant of the spring and η is dynamic viscosity of dash-pot. Stresses are added in case of parallel spring and dash-pot combination. Stress $\sigma(x,t)$ called longitudinal stress and material derivative is used to add the axial effect as follows,

$$\sigma(x,t) = E\epsilon + \eta \frac{\partial \epsilon}{\partial t} + v \frac{\partial \epsilon}{\partial x}. \tag{4.23}$$

Where, ϵ is the nonlinear strain from Equation (4.8).

$$\frac{\partial w}{\partial x}\left(A\sigma \frac{\partial w}{\partial x}\right) = \frac{3EA}{2}\left(\frac{\partial w}{\partial x}\right)^2 \frac{\partial w^2}{\partial x^2} + 2A\eta \frac{\partial w}{\partial x}\frac{\partial w^2}{\partial x^2}\frac{\partial w^2}{\partial x \partial t}$$

$$+ A\eta\left(\frac{\partial w}{\partial x}\right)^2 \frac{\partial w^3}{\partial x^2 \partial t} + 2Av\eta \frac{\partial w}{\partial x}\left(\frac{\partial w^2}{\partial x^2}\right)^2 + Av\eta\left(\frac{\partial w}{\partial x}\right)^2 \frac{\partial w^3}{\partial x^3}. \tag{4.24}$$

The Equation (4.18) is derived and is a second order nonlinear differential equation of motion of a moving elastic string,

$$\rho A\frac{\partial w^2}{\partial t^2}+\rho Av^2\frac{\partial w^2}{\partial x^2}+2\rho Av\frac{\partial^2 w}{\partial x\partial t}-P\frac{\partial^2 w}{\partial x^2}$$

$$-\frac{3EA}{4}\frac{\partial w^2}{\partial x^2}\left(\frac{\partial w}{\partial x}\right)^2+2\mu\frac{\partial w}{\partial t}=\frac{\partial w}{\partial x}\left(A\sigma\frac{\partial w}{\partial x}\right). \tag{4.25}$$

Substituting Equation (4.24) into Equation (4.25), yields the second order nonlinear differential equation of motion for the axially moving viscoelastic string which is,

$$\frac{\partial w^2}{\partial t^2}+v^2\frac{\partial w^2}{\partial x^2}+2v\frac{\partial^2 w}{\partial x\partial t}-\frac{P}{\rho_l}\frac{\partial^2 w}{\partial x^2}+\frac{2\mu}{\rho_l}\frac{\partial w}{\partial t}=\frac{9EA}{4\rho_l}\left(\frac{\partial w}{\partial x}\right)^2\frac{\partial w^2}{\partial x^2}$$

$$+\frac{2A\eta}{\rho_l}\frac{\partial w}{\partial x}\frac{\partial w^2}{\partial x^2}\frac{\partial w^2}{\partial x\partial t}+\frac{A\eta}{\rho_l}\left(\frac{\partial w}{\partial x}\right)^2\frac{\partial w^3}{\partial x^2\partial t}+\frac{2Av\eta}{\rho_l}\frac{\partial w}{\partial x}\left(\frac{\partial w^2}{\partial x^2}\right)^2+\frac{Av\eta}{\rho_l}\left(\frac{\partial w}{\partial x}\right)^2\frac{\partial w^3}{\partial x^3}. \tag{4.26}$$

4.2.1 One term Galerkin discretization of governing equation of axially moving viscoelastic string

Galerkin method is used for discretization and let us recall from Equation (4.20) that,

$$w(x,t)=T_n\sin\left(\frac{n\pi x}{L}\right).$$

Where, $\sin(\frac{n\pi x}{L})$ is first mode shape of vibration for a simply supported stationary string. For one term approximation n = 1,

$$w(x,t)=T\sin\left(\frac{\pi x}{L}\right). \tag{4.27}$$

Substituting Equation (4.27) into Equation (4.26) yields,

$$\sin\left(\frac{\pi x}{L}\right)\ddot{T}+\frac{2v\pi}{L}\cos\left(\frac{\pi x}{L}\right)\dot{T}+\frac{\pi^2}{L^2}\left(\frac{P}{\rho_l}-v^2\right)\frac{\pi^2}{L^2}\sin\left(\frac{\pi x}{L}\right)T$$

$$+\frac{9EA}{4\rho_l}\left(\frac{T\pi}{L}\cos\left(\frac{\pi x}{L}\right)\right)^2\frac{\pi^2}{L^2}\sin\left(\frac{\pi x}{L}\right)T+\frac{2\mu}{\rho_l}\sin\left(\frac{\pi x}{L}\right)\dot{T}$$

$$+\frac{A\eta\pi}{\rho_l L}T\cos\left(\frac{\pi x}{L}\right)T\frac{\pi^2}{L^2}\sin\left(\frac{\pi x}{L}\right)\frac{\pi}{L}\cos\left(\frac{\pi x}{L}\right)\dot{T}$$

$$+\frac{A\eta\pi^4}{\rho_l L^4}T\left(\cos\left(\frac{\pi x}{L}\right)\right)^2\sin\left(\frac{\pi x}{L}\right)T^2\dot{T}=0. \tag{4.28}$$

Multiplying the above equation by first mode shape of vibration and integrating from 0 to L, yields simplified equation as follows,

$$\ddot{T}+\frac{2\mu}{\rho_l}\dot{T}+\frac{\pi^2}{L^2}\left(\frac{P}{\rho_l}+v^2\right)T+\frac{9EA\pi^4}{32L^3\rho_l}T^3+\frac{3A\eta\pi^4}{8L^3\rho_l}T^2\dot{T}=0. \tag{4.29}$$

Solution of substituting Equation (4.29) into Equation (4.27), based on axially moving viscoelastic string is given below, which shows the amplitude time history response of an axially moving viscoelastic string with the influencing parameters of damping, web axial speed and web tension.

It can be concluded from Figure 4.7 that increasing dynamic viscosity will minimize

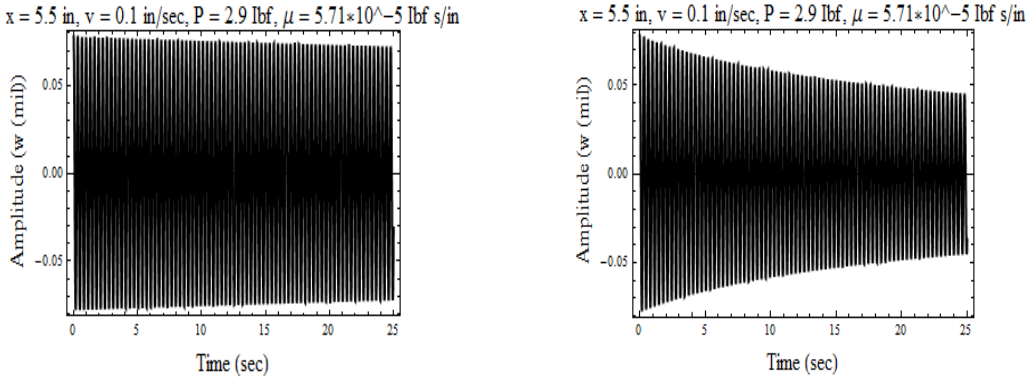

(a) η = 145.038 psi.s (b) η = 2393.123 psi.s

Figure 4.7: Effect of dynamic viscosity on amplitude time history response of viscoelastic string.

amplitude of system response same as that of air damping. In addition to this, the decrease in amplitude means more energy is dissipated which is good, because it is the property of viscoelasticity and can be verified from [25].

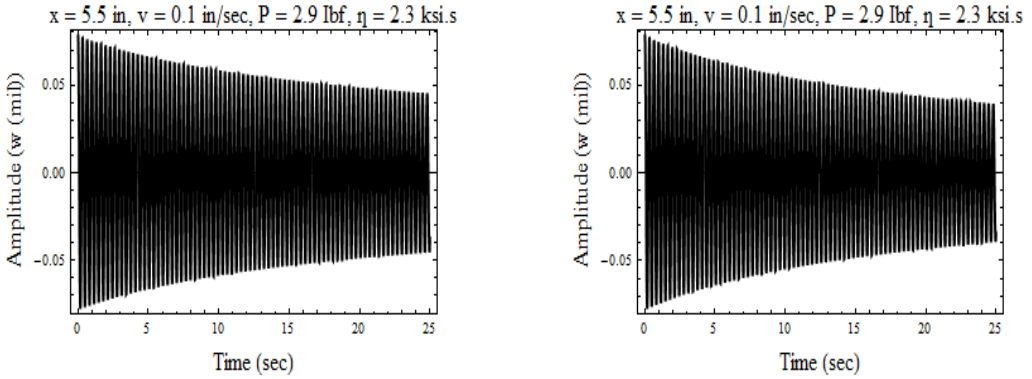

(a) $\mu = 5.71{*}10^{-5}$ (Ibf s/in) (b) $\mu = 5.71{*}10^{-4}$ (Ibf s/in)

Figure 4.8: Effect of air damping on amplitude time history response of viscoelastic string.

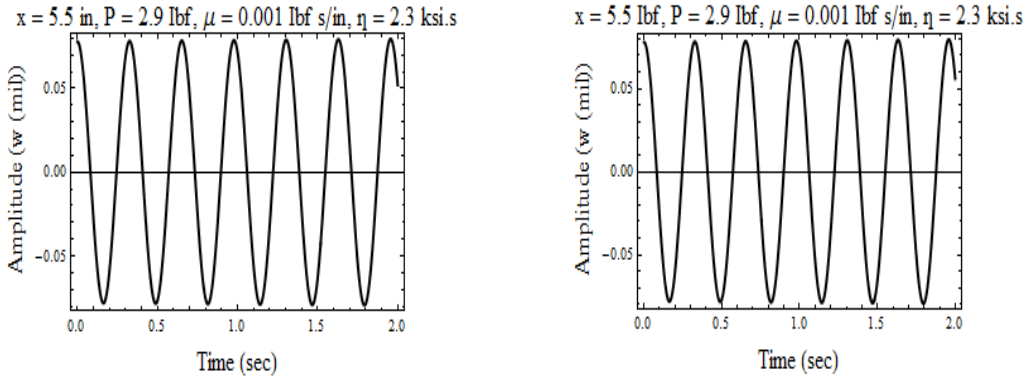

(a) $v = 0.1$ (in/s) (b) $v = 4$ (in/s)

Figure 4.9: Effect of web velocity on amplitude time history response of viscoelastic string.

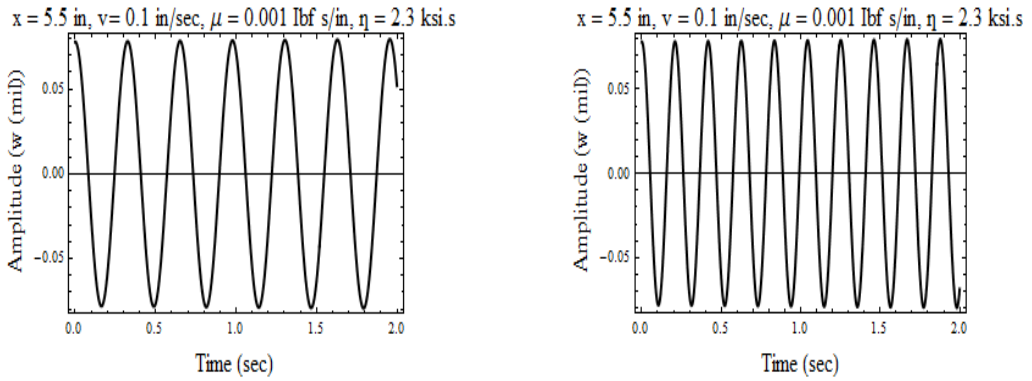

(a) P = 2.9 (lbf) (b) P = 7.1 (lbf)

Figure 4.10: Effect of web tension on amplitude time history response of viscoelastic string.

The effect of air damping is obvious and absorbs energy of vibrations by reducing its amplitude and can be verified from [42]. It can be inferred from Figure 4.8 that increasing air damping will decrease amplitude of time history response of the system for the same viscoelastic web. Therefore, it suggests that viscoelasticity and air damping have the same effect on the response. Effect of web axial speed is analyzed for various axial speeds on amplitude time history response of axially moving viscoelastic string. It is concluded from Figure 4.9 that web axial speed has no significant effect on amplitude time history response and this effect on amplitude time history response can be confirmed from [25]. It can be inferred from Figure 4.10 that web tension increases frequency of amplitude time history response of the moving viscoelastic web.

4.2.2 Frequency of viscoelastic string model using Harmonic Balance Method

Let us consider second order nonlinear differential Equation (4.26). It is assumed that the frequency is harmonic therefore, its amplitude can be presented as,

$$w(x,t) = cos(\omega t)u(x). \tag{4.30}$$

Let, $\omega t = f$ and substituting Equation (4.30) in Equation (4.26) yields,

$$-f^2 u(x)\, cosf - 2vf u_{,x}\ sinf - \left(\frac{P}{\rho_l} - v^2\right) u_{,xx}\, cosf - \frac{2\mu f}{\rho_l} u\,(x)\, sinf =$$

$$\frac{9EA}{4\rho_l}\,(u_{,x})^2\, u_{,xx}\ cos^2 f cosf - \frac{-2A\eta f}{\rho_l}(u_{,x})^2 u_{,xx}\, cos^2 f sinf - \frac{A\eta f}{\rho_l}(u_{,x})^2 u_{,xx}\ cos^2 f sinf$$

$$+ \frac{2A\eta v}{\rho_l}\,(u_{,xx})^2\, cos^2 f - \frac{2A\eta v}{\rho_l}\,(u_{,x})^2\, u_{,xxx}\, cos^3 f. \tag{4.31}$$

Now averaging over one cycle means multiplying the above equation by $cosf$ and integrating this from f 0 to 2π. The simplified resulting equation is a nonlinear second order differential equation for the x-dependent function over $0 \leq x \leq L$,

$$u_{,x}\, f^2 + \left(\frac{P}{\rho_l} - v^2\right) u_{,xx} + \frac{27EA_r}{16\rho_l}\,(u_{,x})^2\, u_{,xx} + \frac{3v\eta}{2\rho_l}\,(u_{,x})^2\, u_{,xx} = 0. \tag{4.32}$$

Now considering the first mode shape of vibration, where A_m is the amplitude of vibration mode is given below,

$$u(x) = A_m sin\left(\frac{\pi x}{L}\right), \tag{4.33}$$

Substituting Equation (4.33) into Equation (4.32), multiplying it by $sin\left(\frac{\pi x}{L}\right)$, integrating from 0 to L and then dividing by 2π yields,

$$f = \frac{\sqrt{\frac{\pi^2}{L^2}\left(\frac{P}{\rho_l} - v^2\right) + \frac{27A_m^2 A_r \pi^4 E}{64\rho_l L^4} + \frac{3vA_m^2 \eta \pi^4}{8L^4 \rho_l}}}{2\pi}. \tag{4.34}$$

Finally Equation (4.34) is obtained which is the frequency equation for a viscoelastic moving web and dividing this by 2π converted it into Hz. A_m can be represented as $A_m = \frac{La}{\pi}$ where a is called harmonic coefficient and A_r is cross sectional area of the string. Equations (4.42), (4.47) and (4.34) can be compared for linear elastic, nonlinear elastic and viscoelastic webs frequency respectively as shown in Figure 4.11.

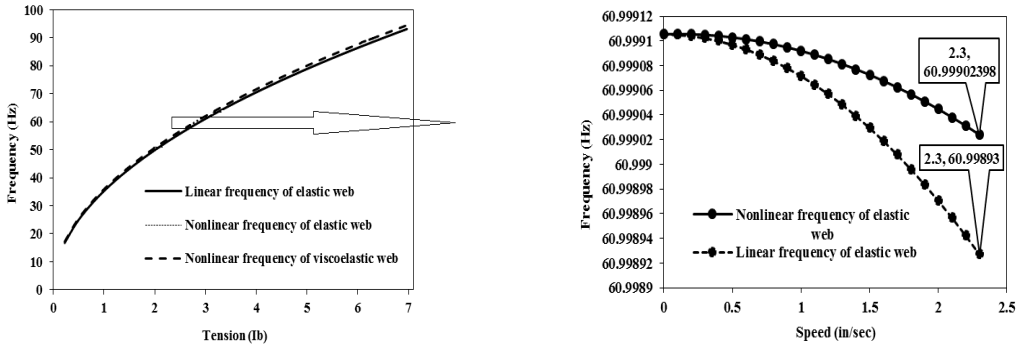

(a) $\eta = 2393.123$ ksi.s (b) $\eta = 145.038$ ksi.s

Figure 4.11: Effect of tension and axial speed on frequency.

These plots are based on a 3 mil thick web moving with an axial speed of 0.1 in/sec. From the Figure 4.11a and Figure 4.11b it is clear that frequency of viscoelastic moving web has same behavior as elastic one with the web transmitted tension. The effect of dynamic viscosity on web frequency is quite small therefore, little decrease is shown in Figure 4.11b. The effect of high dynamic viscosity value on the speed verses frequency can be seen in Figure 4.12, thus concluded negligible effect on web vibration frequency.

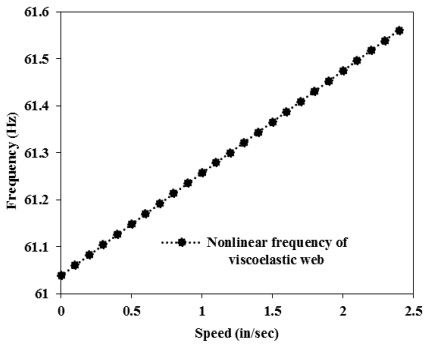

Figure 4.12: Effect of dynamic viscosity $\eta = 2393.123$ ksi.s on speed verses frequency.

In this model two new Equations (4.47) and (4.34) are derived for web frequency and their results can be compared to the Equation (4.42) based on linear elastic web model and finally the results were found to be in good agreement [6, 45]. This also allows us to use the elastic moving string model into the viscoelastic web experimental

results.

4.3 Analytical solution of frequency analysis for elastic string

Second order nonlinear partial differential equation of motion for the moving web is,

$$\rho A\frac{\partial w^2}{\partial t^2}+\rho Av^2\frac{\partial w^2}{\partial x^2}+2\rho Av\frac{\partial^2 w}{\partial x\partial t}-P\frac{\partial w^2}{\partial x^2}$$

$$-\frac{EA}{4}\frac{\partial w}{\partial x}\left(\left(\frac{\partial w}{\partial x}\right)^2\left(\frac{\partial w}{\partial x}\right)\right)+2\mu\frac{\partial w}{\partial t}=0. \tag{4.35}$$

Where, A is string cross-sectional area and ρ_v is mass per unit volume. Dropping damping and nonlinear terms due to which the above equation becomes as follows,

$$\frac{\partial w^2}{\partial t^2}-\left(\frac{P-\rho_v v^2}{\rho A}\right)\frac{\partial w^2}{\partial x^2}+2v\frac{\partial^2 w}{\partial x\partial t}=0$$

$$\frac{\partial w^2}{\partial t^2}+2v\frac{\partial^2 w}{\partial x\partial t}=\left(s^2-v^2\right)\frac{\partial w^2}{\partial x^2}. \tag{4.36}$$

It is a hyperbolic equation where, $\rho_l=\frac{\rho_v}{\rho A}$ is mass per unit length and $s=\sqrt{\frac{P}{v}}$ is called wave velocity. Measured by stationary observer, a material particle on traveling string experiences local, Coriolis and centripetal acceleration components $w_{,tt}$, $2vw_{,xt}$ and $v^2w_{,xx}$ respectively. Analytical solution of the above equation is,

$$w=D_1\sin w\left[t+\left(\frac{\rho v+\sqrt{\rho P}}{P-\rho v^2}\right)x\right]+D_2\sin w\left[t+\left(\frac{\rho v-\sqrt{\rho P}}{P-\rho v^2}\right)x\right]. \tag{4.37}$$

Applying the boundary conditions of $w=0$, at $x=0$ *and* $x=l$ to Equation (4.37) yields Equation (4.38) and Equation (4.39) respectively,

$$D_1+D_2=0, \tag{4.38}$$

$$D_1 \sin w \left[t + \left(\frac{\rho v + \sqrt{\rho P}}{P - \rho v^2} \right) l \right] + D_2 \sin w \left[t + \left(\frac{\rho v - \sqrt{\rho P}}{P - \rho v^2} \right) l \right] = 0, \tag{4.39}$$

The simplification of Equation (4.39) yields,

$$w \left(\frac{\rho v + \sqrt{\sqrt{\rho P}}}{P - \rho v^2} \right) l = w \left(\frac{\rho v - \sqrt{\rho P}}{P - \rho v^2} \right) l + 2\pi n,$$

$$f = \frac{\omega}{2\pi}. \tag{4.40}$$

Substituting Equation (4.40) into simplified Equation (4.39), results in moving web frequency is,

$$f = n \left(\frac{P - \rho v^2}{2l\sqrt{\rho P}} \right). \tag{4.41}$$

For a stationary web, the speed v becomes zero and the above equation simplifies to,

$$f = \left(\frac{nP}{2l\sqrt{\rho P}} \right). \tag{4.42}$$

Using Equation (4.41) the relationship between web tension, axial speed and frequency is plotted for various thicknesses in the following Figure 4.13, using parameters of L = 11 in, width = 4.25 in, web density $\rho = 0.05022$ Ibm/in^3, area A = 0.0063 in^2, 0.0127 in^2, 0.0212 in^2, 0.0296 in^2, speed $v = 0.1$ in/sec and tension T = 6.7 Ibf.

It can be concluded from Figure 4.13 that web with high thickness will vibrate with low frequency by increasing web tension as compared to the low thick web. Similarly, from Figure 4.14a and Figure 4.14b it can be inferred that web with high thickness value will vibrate with low frequency by increasing the web axial speed as compared to the low thick web. The behavior of frequency with web tension and axial speed can be verified from [45].

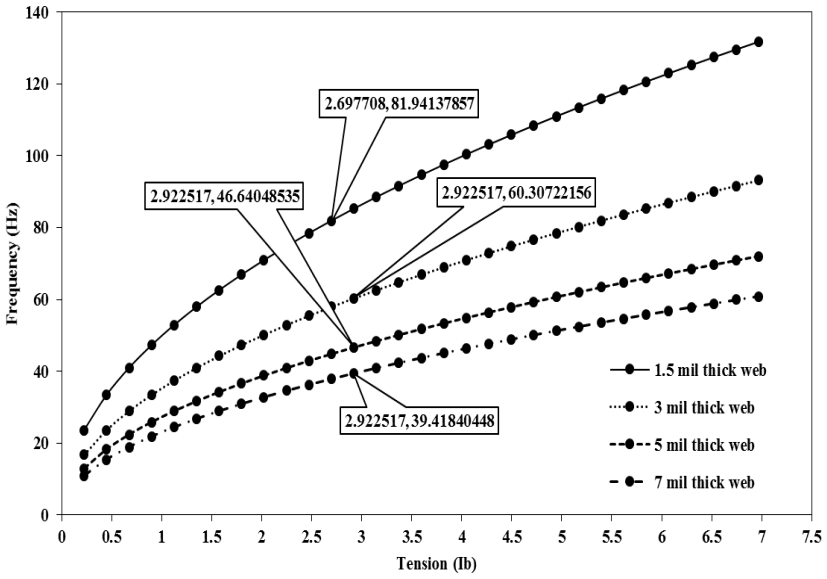

Figure 4.13: Effect of web tension on frequency for various web thicknesses.

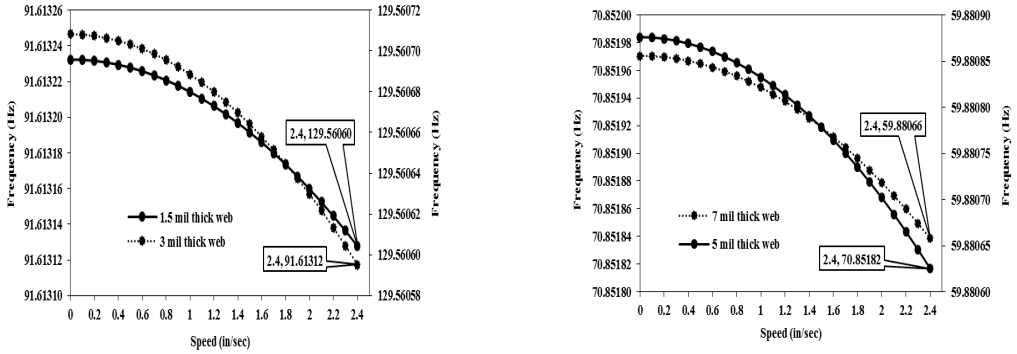

(a) (b)

Figure 4.14: Effect of web axial velocity on frequency for various web thicknesses.

4.3.1 Frequency of elastic string model using Harmonic Balance Method

Let us consider second order nonlinear differential Equation (4.18) which is the governing equation of motion of the moving web. It is assumed that the frequency is

harmonic therefore, its amplitude can be presented as,

$$w(x,t) = cos\omega t\ u(x). \tag{4.43}$$

Let $\omega t = f$ and substituting Equation (4.43) into Equation (4.18) yields,

$$-f^2 u(x) cosf - 2vf u_{,x}\ sinf + \left(v^2 - \frac{P}{\rho_l}\right) u_{,xx}\ cosf$$

$$-\frac{3EA}{4\rho_l}\left(u_{,x}\right)^2 u_{,xx}\ cos^2 f cosf - \frac{2\mu f}{\rho_l} u\left(x\right) sinf = 0. \tag{4.44}$$

Now averaging over one cycle, i.e. multiplying Equation (4.44) by $cos(f)$ and integrating this f from 0 to 2π. The simplified resulting equation is a nonlinear second order differential equation for the x-dependent function over $0 \leq x \leq L$,

$$u_{,x}\, f^2 + \left(\frac{P}{\rho_l} - v^2\right) u_{,xx} + \frac{9EA}{16\rho_l}\left(u_{,x}\right)^2 u_{,xx} = 0. \tag{4.45}$$

By considering the first mode shape of vibration, where A is the amplitude of vibration mode and is given below,

$$u(x) = A_m sin\left(\frac{\pi x}{L}\right). \tag{4.46}$$

Substituting Equation (4.46) into Equation (4.45), multiplying it by $sin\left(\frac{\pi x}{L}\right)$, integrating from 0 to L and dividing by 2π yields,

$$f = \frac{\sqrt{\frac{\pi^2}{L^2}\left(\frac{P}{\rho_l} - v^2\right) + \frac{9A_m^2 A_r \pi^4 E}{64\rho_l L^4}}}{2\pi}. \tag{4.47}$$

The above equation is the frequency equation for moving elastic web and dividing by 2π converted it into Hz. A_m can be represented as $A_m = \frac{aL}{\pi}$, where a is called harmonic coefficient and A_r is cross sectional area. In addition to this, frequency of web transverse vibration increases with the increase of harmonic coefficient as reported

in [46] and can be obtained here as well. Equations (4.47) and (4.42) can be compared for linear and nonlinear frequency shown in Figure 4.15a and in Figure 4.15b.

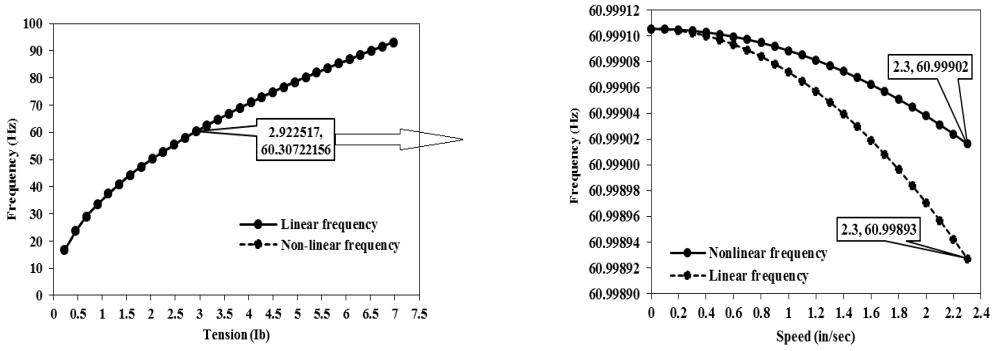

(a) (b)

Figure 4.15: Effect of web tension and axial speed on frequency.

These plots are based on a 3 mil thick web moving with an axial speed of 0.1 in/sec for web tension verses frequency relationship. From Figure 4.15a and Figure 4.15b it is clear that linear and nonlinear frequency of elastic moving web is same for both cases tension verses frequency and axial speed verses frequency, thus can be verified from Comsol simulations as well.

4.4 Numerical solution of frequency analysis using Comsol

Frequency depends on both web tension and axial speed. But in the analytical solutions for both elastic and viscoelastic web, vibration frequency is highly affected by web tension as compared to the axial speed shown in Figure 4.16a and Figure 4.16b.

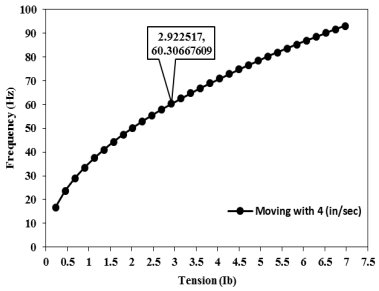

(a) Moving web.

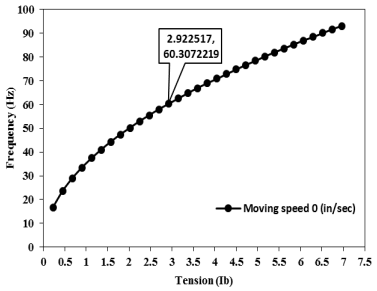

(b) Stationary web.

Figure 4.16: Effect of web axial speed on tension verses frequency.

For both moving (4 in/sec) and non-moving cases the web frequency at 6.7 Ibf web tension is 91.6 Hz. From both plots, it is concluded that axial speed is less important for frequency because the axial speed has a very small effect on the web frequency. Due to this reason Comsol simulations for web frequency are carried out for a stationary string and thin plate models to validate the analytical solutions results.

4.4.1 Frequency of a string model

In this model the natural frequencies of a pretensioned string using 2D truss interface are computed and representing "stress stiffening". In fact, transverse stiffness of truss elements is directly proportional to tensile force. Strings made of piano wire have an extremely high yield limit thus enabling a wide range of pretensioned forces. The results can be compared with the analytical solutions of axially moving elastic and viscoelastic strings. Let us consider the following data for Comsol simulations:

- (a) Geometry:
  - String length $L = 11$ in
  - Cross-sectional area of the string = $A = 0.0127$ in^2
- (b) Material:
  - Young's modulus $E = 725188$ psi

* Poisson's ratio $\nu = 0.38$
* Mass density $\rho =!0.05022$ Ibm/in^3

- (c) Constraints:

  The string is simply supported i.e. pinned at both ends.

- (d) Load:
  * The wire is pretensioned to $\sigma_{ni} = 529387$ psi.

Web frequency for first mode shape of vibration is obtained from analytical solution for 6.7 Ibf force is 91.6 Hz. Frequency result is obtained in Comsol as shown in Figure 4.17, which verifies the analytical models and web vibration frequency for linear, nonlinear and viscoelastic string models is very close to 91.6 Hz at 6.7 Ibf web tension force.

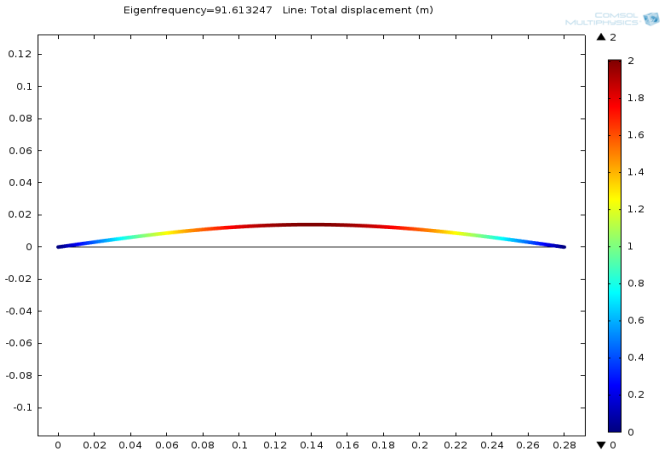

Figure 4.17: Web vibration frequency.

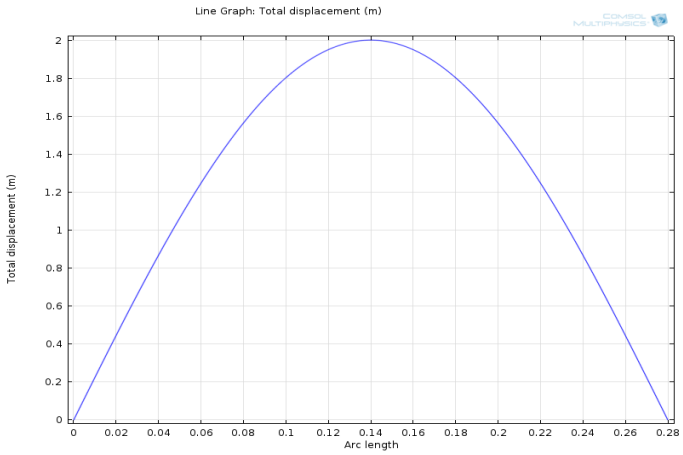

Figure 4.18: First eigen mode shape.

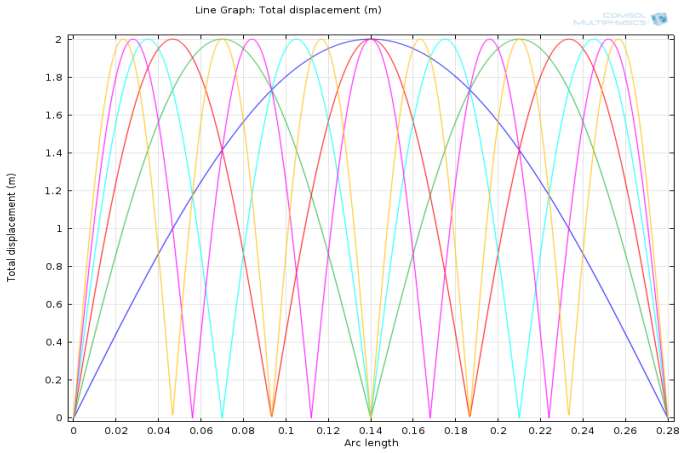

Figure 4.19: First six eigen mode shapes.

Finally Figure 4.18 and Figure 4.19 represent vibration mode shapes of a stationary string model where Figure 4.18 represents only the first mode shape of vibration and second one represents all the six modes of vibration respectively. As the stresses are known in advance, therefore it is possible to use an initial stress condition.

4.4.2 Frequency of a thin plate model

The same analysis was performed for a stationary thin plate model in Comsol. Membrane is also called thin plate and it is interesting that results found, are very close to the stationary string model. Thin plate is pinned at both ends and same initial stress

is applied. The pinned boundary conditions have been used for both string and thin plate models because in case of simply supported or pinned boundary conditions, the displacement at x = 0 and x = L is zero, which were used in analytical and numerical models to give the same frequency results. Therefore web vibration frequency results can be seen in Figure 4.20a, Figure 4.20b and Figure 4.20c.

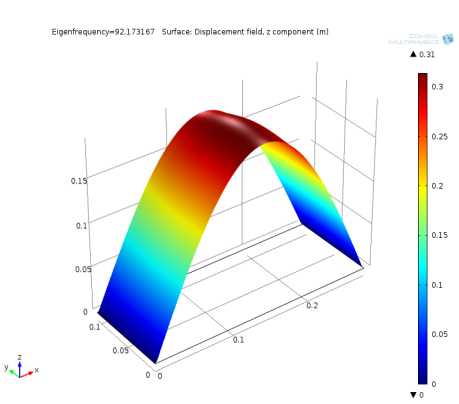

(a) 3 mill thick web.

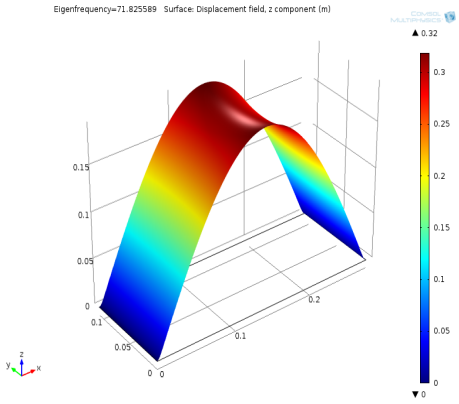

(b) 5 mill thick web.

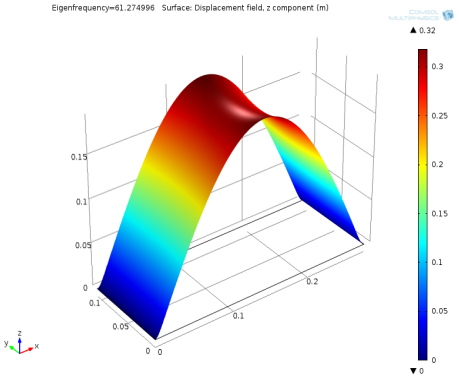

(c) 7 mil thick web.

Figure 4.20: Tension verses frequency for various thicknesses of a thin plate web.

Where web frequency at 6.7 Ibf web tension and for 3 mil web is 92.17 Hz, 5 mil is 71.82 Hz and 7 mil is 61.27 Hz respectively. From all these plots in Figure 4.20a, Figure 4.20b and Figure 4.20c we can also conclude that web with a high thickness will vibrate with a lower web frequency and results are in good agreement with analytical solutions for axially moving elastic and viscoelastic string models.

CHAPTER 5

EXPERIMENTAL INVESTIGATION OF TRANSVERSE VIBRATION OF AXIALLY MOVING PET WEB

The purpose of this chapter is to describe the equipments and its use for the experimental setup. In the setup, displacement sensor is used to find the vibration frequency of a moving PET web.

5.1 Equipment description

5.1.1 Micro-measurement displacement system (muMDS)

muDMS is a measuring system used for small displacements and based on D-type and RC-type fiber-optics which provide linear output of the measured distance using USB 2.0 protocol and consists of:

1. Reflectance compensated fiber-optic bundles which is used for measuring analogue input signals.

2. A digital processing unit with a storage capacity of 25 calibrations.

3. A mini-USB connector is used for USB output.

4. An adapter cable used to connect standard USB to mini-USB.

5. An alternating and direct current (AC/DC) power supply of 12 volts with a current of 350 mA and a weather-tight connector.

5.1.2 Sensor fiber optic probes

There are two types of fiber-optic probes D and RC models. D-types have random mixture of transmitting and receiving fibers which are always round bundles. While RC-models are made of round and rectangular fiber-optic bundles. D-type sensors are reflectance compensated and mainly used for one dimensional measurements where the target reflectivity is not changing. RC-types sensors are used for measuring translation and rotation motion of the target with varying surface reflectivity.

5.1.3 Reflectance compensated model operating principle

Operating principle is explained as follows:

1. One fiber-optic bundle is used to send light to the target surface while the other two bundles are used to receive light reflected back from the target surface.

2. Transmit bundle is randomly mixed with one receiver bundle in the probe tip.

3. The two receiver bundles are mixed adjacent to one another.

4. In the two receivers light intensity is processed ratio-metrically in the DMS compared with 24 bit resolution to store calibration data.

5. This ratio-metric function provides measured distance which is not depending on changing reflectance of the target surface.

6. For best operation, sensor tip should be clean and clear. Accurate value of the amplitude depends upon precise reflection of rays from the target surface. Alcohol, soft cloth and tissue can be used for cleaning the sensor tip.

5.1.4 Sensor tip alignment

In Figure 5.1 a displacement sensor, its axes and alignment flat can be seen:

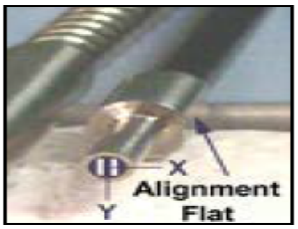

Figure 5.1: Sensor alignment illustration [47].

1. Flat on sensor casing is used to help in alignment and is parallel to fiber-optic bundles split on sensor face.

2. Tip alignment depends on the applications, like for a cylindrical target x-axis, tip should be parallel to the cylindrical axis.

3. Sensor x-axis should be parallel to the direction of motion.

4. It is 10 times more sensitive if tilt about y-axis than x -axis. Therefore, align the target surface parallel to the sensor x-axis.

5. Alignment is easy for smooth and flat surfaces.

6. Tip of the sensor should be perpendicular to the target surface.

5.1.5 Calibration, communication and temperature stabilization of the sensor

There are two factory calibrations for each sensor channel a mirrored and diffuse target, for which up to 25 calibrations can be stored. USB port is used for communication and DMS pin 2 and 3 are used for transmitting and receiving purposes. For temperature stabilization power is supplied and amplifier is allowed to reach thermal equilibrium in about 30 min or less. Then set temperature is increased 2 to 3 degrees above equilibrium and finally amplifier temperature is maintained which only fluctuate within $\pm$ 0.1 ^0C.

5.1.6 Operating range of the sensor

Sensor should be placed within the operating range for optimum measurements. Sensor is positioned, where signal to noise ratio is high i.e. where RC-function has steepest slope. For each sensor, a sensitivity chart is given in [47], which shows the relation between RC-function vs. Distance. Each sensor is calibrated with a 0.007 mil accuracy of a linear air bearing stage. Custom calibration can be done by moving the target from stationary sensor with small steps and then bringing to its original position with the same steps.

Mirror calibration is used for smooth, polished, glossy and mirrored surfaces while diffuse calibration is used for dull surfaces. If diffuse calibration is not working, then calibrate your system according to the following relative reflectance of some common materials in Table 5.1.

Table 5.1: Relative reflectance [47].

Material	% Reflectance
Gold Mirror	100
Mirror Polished Aluminum	85-90
Mirror Polished Stls Stl	60-70
Brushed Aluminum	40-50
Copper Clad PC Board	45
Finely Ground Steel	30-35
Anodized Aluminum	20-25
Silver Paint, Glossy	15-20
Photo Paper, High Gloss	15
Inkjet Paper, Bright White	7-8
Fiberglass, Glossy	7
Black Plastic, Glossy	6
Black Matte Finish	3
Column of Water	2
Flat Black Rubber	1

5.1.7 Operation of the sensor

Install DMS control software on the PC and execute it which reads all the calibrations table from the sensor. Open tab from single channel tab for a USB sensor and select its serial number from the top down list. After reaching sensor to thermal equilibrium, it is ready to collect measurement data and use DATA STREAM tab for high speed data measurement. There are different tabs and options in the control software for good operation and for low data stream, a live plot is shown. But the important point is that its capacity to show live plot of displacement is up to 60 samples/second which is due to buffering limit. High stream data can't be observed due to this limitation, but in saving the high speed data is accurate and no issue can be observed. For detailed operation procedure please refer to manual of muDMS RC-100 PHILTEC sensor [48].

5.2 Micro-displacement measurement system reflectance compensated-100 sensor

muDMS RC-100 is a displacement sensor for measuring distance, displacement and vibration of a target surface. It is manufactured by PHILTECT incorporation and fiberoptics cable, sensor with a control DMS system is shown in Figure 5.2.

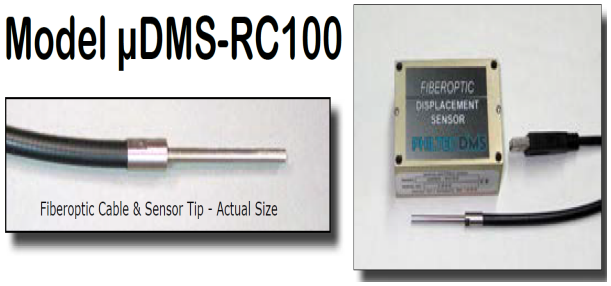

Figure 5.2: For distance, displacement and vibration measurement [48].

The features of muDMS RC-100 sensor are shown in Figure 5.3.

1. Output is reflectance compensated.
2. Ø is the spot size and is equal to 98.5 mil.
3. Operating range 200 mil and Linear range 80 mil.
4. 1.3 mv/0.040 mil sensitivity is 33 mv/mil.

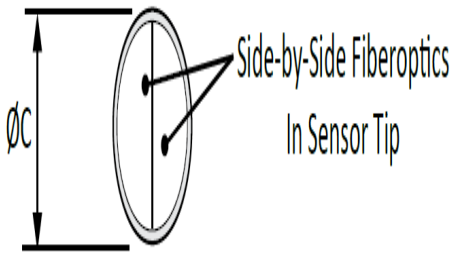

Figure 5.3: Features of the sensor tip [48].

The features of muDMS RC-100 sensor tip and cable which includes tip, collar, cable length and their dimensions are given in [48]. Signal is reflected from the target and received by the sensor. Then it is processed and converted to distance by using ratiometric calculation and stored by on-board sensor. Sensor can be gapped within the operating range. Optimum performance is obtained if the sensor is gapped within 39.4-196.85 mil range where the sensitivity is high and RC function has steepest slope as shown in Figure 5.4,

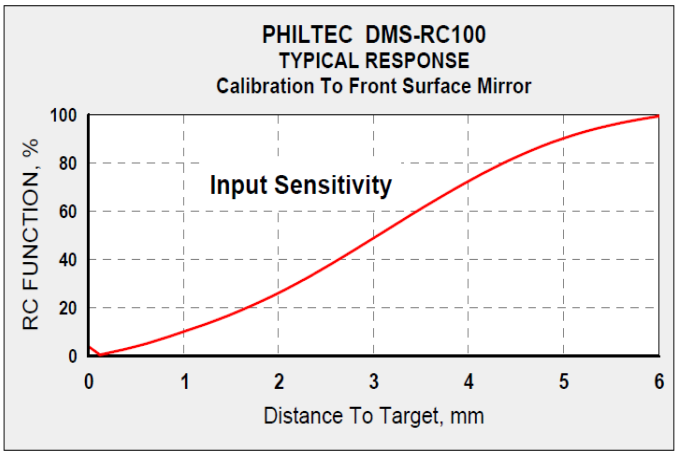

Figure 5.4: Typical response of muDMS RC-100 sensor.

where detailed standards specifications (electronics, fiberoptics and USB output) of the sensor are given in [48]. These specifications represent the best case performance where:

1. The Target surface is straight, smooth and highly reflective.
2. Sensor tip is perpendicular to the target surface.
3. Sensor is placed within the operating range of high sensitivity.
4. Cable lengths are standard and cannot be connected to other cables.

5.3 Experimental setup of micro-displacement measurement system reflectance compensated-100 sensor

The displacement sensor is installed on roll-to-roll web system platform and experiments are conducted to measure amplitude of web flutter as shown in Figure 5.5, where various parts of experimental setup are presented. This sensor has much better resolution of 0.007 mil as compared to the one discussed in [32]. This sensor has a range of 200.7 mil, linear range of 82.6 mil and a Light Emitting Diode (LED) source of light having a wavelength of 0.0340 mil. The reflected light is received by two receiver bundles and its intensity depends upon the material surface where mirrored or polish surface easily gives high signal to noise ratio (SNR). The transmitted power for all applications is 100 % and receiver power is dependent on surface reflectance and adjustment of sensor position in the operating range.

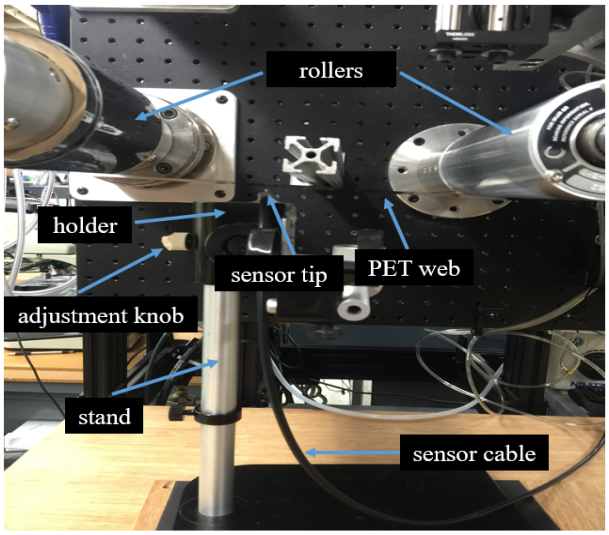

Figure 5.5: Roll-to-roll platform for displacement sensor setup.

The transverse vibration is measured by using the displacement sensor with a sampling rate of 651 Hz (muDMS RC-100 Sensor). The measurement acquisition is

performed using DMS control software based on LabVIEW coding through USB port. In software, live data can be seen as well it can be saved in filename.txt files. These filename.txt extension files are then imported to Matlab and Fast Fourier transform algorithm is used to find web fluttering frequency from recorded data. Sensor records the data in millimeter or micrometer and are provided by the DMS control software. For calibration mirrored surface is used which is factory based setting and its accuracy is up to 0.007 mil.

5.4 Experimental results using displacement sensor

In all these experiments PET is used as a web which passes over two rollers. It unwind the web from one roller and rewind it on another roller. The micro-contact printing machine is run at various web axial speeds from 0 to 4 in/sec and applied different tensions from 3 to 9 Ibf to perform all the required experiments. The parameters of PET used in the experiments are its length is 11 in, width is 4.5 in and thickness is 1.5 mil.

In the following plots 1000 data points are collected from the fluttering web which are shown in Figure 5.6a and after this FFT algorithm is used to determine frequency of fluctuation which is called frequency of displacement as shown in Figure 5.6. Similar analysis are done, to find frequency of velocity and acceleration by converting displacement data to velocity and acceleration as shown in Figure 5.6a.

Particularly an experiment is performed at 3 Ibf web tension with a stationary case for a 1.5 mil thick web. For a 3 Ibf web tension the web fluttering frequency should be 79.5 Hz from Equation (4.41) as compared to 79.99 Hz experimental value . At 4 Ibf it should be 70.9 Hz analytically as compared to 68.29 Hz experimental value. These results are in good agreement with the analytical ones and can also be seen in the following Figure 5.6. These results are taken from positive direction of machine

which is counter clockwise.

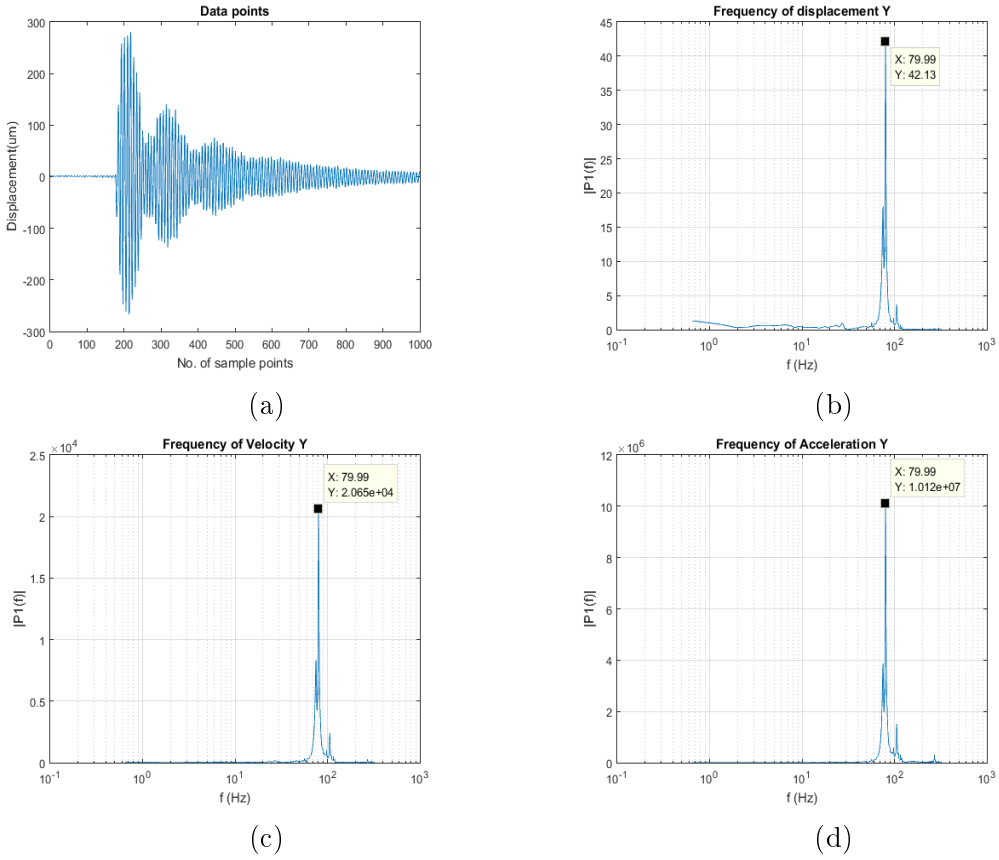

Figure 5.6: Frequency analysis using FFT algorithm.

Based on the above analysis, a series of experiments are performed to established a relationship between web transmitted tension and frequency. The results are shown in Figure 5.7, which verifies that at 0 in/sec axial speed the results are in very good agreement for both experimental and analytical cases.

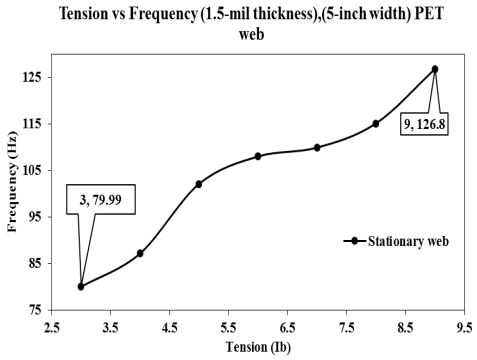

Figure 5.7: Effect on web vibration frequency with the variation of web transmitted tension

Now another experiment is performed with a 3 mil thick and 4.25 in wide web. From analytical solution for this case of 3 lbf web tension, the frequency should be 61.3 Hz as compared to 54.63 Hz experimental value. In the same manner, at 7 lbf analytically frequency should be 91.6 Hz as compared to 93 Hz experimental one. It can be seen that the difference is very low between the frequencies at high web tension. All the results are plotted as follows in Figure 5.8.

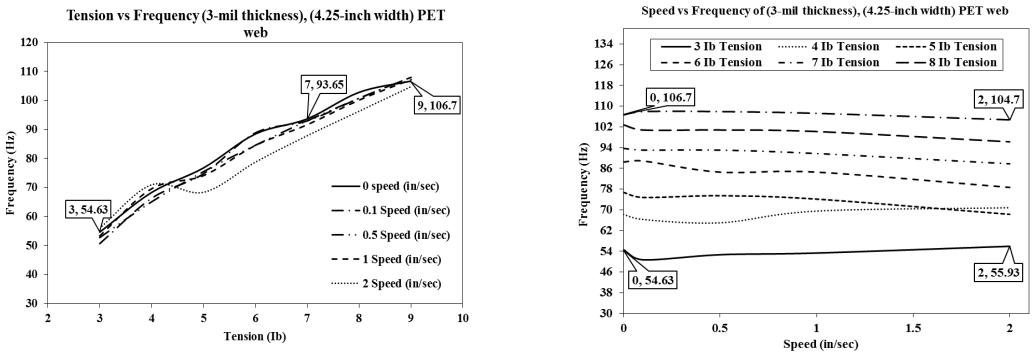

(a) (b)

Figure 5.8: Effect on web vibration frequency with the variation of web transmitted tension and axial speed.

From analytical solution between the web axial speed and frequency at 9 lbf and 0 in/sec, frequency is 106 Hz as compared to 104.7 Hz from experimental data which shows that web fluttering frequency is relatively less affected by web axial speed than

transmitted tension. This variation of web vibration frequency with the axial speed cannot be verified from the analytical model, as in analytical model web vibration frequency varies slightly with the web axial speed. This kind of behavior was also observed by [6] using laser sensor for web frequency determination. Now this experiment is performed with a 5 mil thick and 4.25 in wide web. For an axial speed of 0.1 in/sec analytical frequency is 46.64 Hz at 3 Ibf as compared to 47.48 Hz for the same axial speed. Furthermore, frequency at 7 Ibf is 72.02 Hz experimentally for an axial speed of 0.1 in/sec as compared to the analytical result which is 75.44 Hz. It can be concluded that the results are still good and are presented in Figure 5.9a.

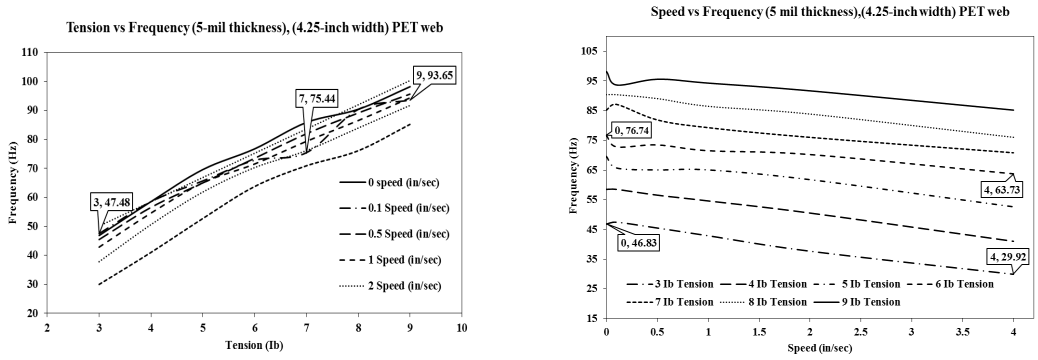

(a) (b)

Figure 5.9: Effect on web vibration frequency with the variation of web transmitted tension and axial speed.

From web axial speed verses frequency plot in Figure 5.9b, it can be seen that for a 3 Ibf web tension, the difference in frequencies is about 17 Hz because at 0 in/sec the frequency is 46.83 Hz as compared to 29.92 Hz at 4 in/sec. But at high web tension of 9 Ibf, frequency is 98.2 Hz at 0 in/sec as compared to 29.92 Hz at 4 in/sec and the difference is about 13 Hz. It is observed from these results that at high web tension, web frequency difference is small for the same number of two axial speeds at 0 and 4 in/sec.

This final experiment is performed for 7 mil thick and 4.25 in wide web shown in Figure 5.10. For thick web high web tension is required to stretch it properly and make

it movable on roll-to-roll machine. When the web thickness increases, web frequency should decreases and it is also happening here. For a 7 mil thick web at 0 in/sec axial speed and 3 Ibf web tension, web frequency should be equal to 40 Hz analytically as compared to 40.76 Hz experimental result. Similarly, at 7 Ibf it must be analytically 61 Hz as compared to 61.65 Hz the experimental result. It can be inferred that analytical and experimental results are in good agreement. All experimental results cannot be verified form the analytical solution due to different factors but many of the results can be calculated and verified. In addition to this, it is advisable to use high web tension forces for thick web to achieve a good properly axially moving web.

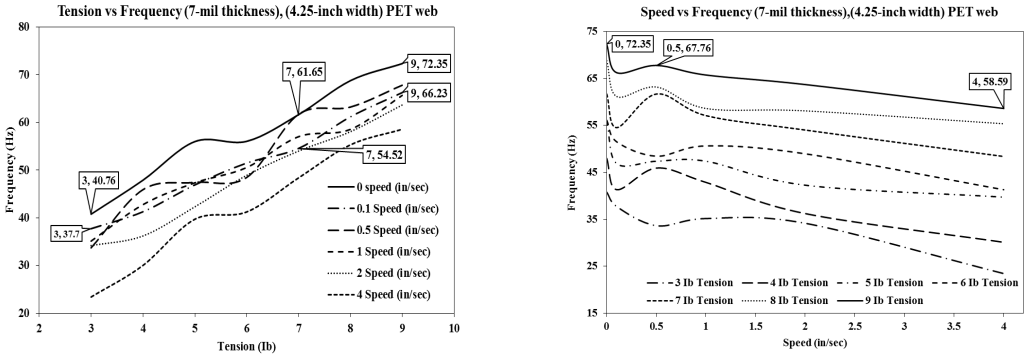

(a) (b)

Figure 5.10: Effect on web vibration frequency with the variation of transmitted tension and axial speed.

From web axial speed and frequency relation it is clear that frequency decreases with the increase in web axial speed. From the plots, all curves in the start are not smooth and behaving differently, one of the reason for this could be that machine is not properly working at low web tensions. For example, while working on machine if web tension is less than 3 Ibf, machine will not even move. At 9 Ibf tension and 0 in/sec axial speed, frequency is 72.35 Hz as compared to the same conditions and changing axial speed to 4 in/sec, web frequency decreases to 58.59 Hz which shows high dependency of frequency on web axial speed.

This procedure can be performed by using only one sensor (a displacement sensor

and combination of wound and unwind rollers that are currently available on electrical servo motors of machine) and other data are computed from sensor-measured data. It is also possible to use additional sensors that may also be in operation with winding and unwinding machine. In this case, it is necessary to choose during implementation of web transmitted tension procedure between measured data and computed ones and then employ data fusion. A number of difficulties faced are:

1. There could be a chance of interference between free and force vibrations and their separation is not an easy task.

2. The web frequency is influenced by web axial speed, therefore it is more important to consider high velocities relation with web frequency.

3. For large-width webs, model of a vibrating string or beam with low rigidity may no longer be valid. In this case, model of a moving three dimensional membrane, should be more appropriate for dynamic analysis.

4. The important thing is real value of tension in the web, as currently there is no controller or measuring sensor which can actually provide exact value of the transmitted web tension. Therefore, there are few values which cannot be verified exactly from analytical solution.

5. Another important fact about micro-contact printing machine is that, it could not move for a web tension less than 3 Ibf. Thus, it means that the force applied through LabVIEW program to servo motors does not mean that same force is applied on the web. There might be some inertial and friction torques losses which are affecting results.

6. Furthermore, sampling rates are verified from the companies but sensor does not give exact sample rates and by changing sampling rate in Matlab algorithm, numerous variations in results occur. For 7 mil thick web the sampling rate of

510 is used which gives quiet good results instead of 651 Hz. The reason for this is that, the recorded data is compared from txt file to the actually recorded data by the sensor is 510 sample per second.

CHAPTER 6

CONCLUSIONS & RECOMMENDATIONS

Micro-contact printing is an emerging technology where roll-to-roll dynamics and web vibrations play a key role in printing quality of the features. Therefore, it is of vital importance to develop a new mathematical model and investigate the effects of different parameters on system's dynamics and web flutter. Furthermore, experimental work provides a strong support to the analytical model by utilizing a novel displacement sensor. PET web was characterized at room temperature, thus confirming its viscoelastic behavior. Furthermore, transverse vibration of a PET web was investigated both analytically and experimentally based on an axially moving string model. The governing equation of motion for the moving web was derived by using Hamilton's principle. The Kelvin-Voight viscoelastic model was successfully introduced into the mathematical model. Galerkin method was employed for discretization of the governing equation of the moving web. Dynamic response of the web is analyzed by determining influence of web axial speed and transmitted tension, web viscoelasticity and surrounding air damping induced. Therefore, it could be inferred that dynamic response was affected more by transmitted tension as compared to the web axial speed. Furthermore, air damping and dynamic viscosity of the dash-pot tend to minimize the amplitude of vibrations. Second

order differential nonlinear equation of motion for elastic web was linearized and solved for web vibration frequency equation. In addition to this, the second order differential nonlinear equation of motion was solved by Harmonic Balance Method and web vibration frequency equation was derived for both elastic and viscoelastic model of the web. Three different frequency relationships were derived from linear, nonlinear and viscoelastic equation of motion and it was observed that all of the relationships provided quite similar results. For validation of frequency equation results, simulations were carried out on Comsol for a stationary string and thin plate models, and results are found to be in good agreement with the analytical ones. Finally, a novel displacement sensor was utilized to measure web vibration amplitude. A Fast Fourier Transform algorithm was used to obtain web vibration frequency for axially moving webs. Thus, analytical and experimental results were found to be in good agreement for web tension influence on web frequency while experimental results also show stronger effect of web axial speed on web frequency than the analytical string model.

Possible recommendations for the future work could be:

- The mathematical model derived can be modified to consider the effects of varying tensions and speeds.
- The equation of motion could be solved for other boundary conditions than the simply supported one.
- The effect of roller inertia, motor torque and varying radii could be introduced to consider a more realistic model.

REFERENCES

[1] A.Kumar and G.Whitesides, "Features of gold having micrometer to centimeter dimensions can be formed through a combination of stamping with an elastomeric stamp and an alkanethiol ink followed by chemical etching," *Apply. Phys*, vol. 63, no. 14, pp. 2002–2004, Oct. 1993.

[2] A. A.Kumar and M.Whitesides, "Features of gold having micrometer to centimeter dimensions can be formed through a combination of stamping with an elastomeric stamp and an alkanethiol ink followed by chemical etching," *Apply. Phys*, vol. 10, no. 5, p. 1498–1511, May 1994.

[3] A. M. Libert, "Precision control of cylindrical stamp contact in a continuous roll-to-roll micro-contact printing machine," *Master Thesis*, pp. 42–43, Jun. 2014.

[4] A. Perl, D. N. Reinhoudt, and J. Huskens, "Microcontact printing: limitations and achievements," *Advanced Materials*, vol. 21, no. 22, pp. 2257–2268, 2009.

[5] A. P. Quist, E. Pavlovic, and S. Oscarsson, *Analytical and bioanalytical chemistry*, vol. 381, no. 3, pp. 591–600, 2005.

[6] M. Vedrines, V. Gassmann, and D. Knittel, "Moving web-tension determination by out-of-plane vibration measurements using a laser," *Instrumentation and Measurement, IEEE Transactions on*, vol. 58, no. 1, pp. 207–213, 2009.

[7] A. Ulsoy, C. Mote Jr, and R. Szymni, "Principal developments in band saw vibration and stability research," *Holz als Roh-und Werkstoff*, vol. 36, no. 7, pp. 273–280, 1978.

[8] J. Wickert and C. Mote, "Travelling load response of an axially moving string," *Journal of Sound and Vibration*, vol. 149, no. 2, pp. 267–284, 1991.

[9] J. Wicker and C. Mote Jr, "Current research on the vibration and stability of axially-moving materials," *The Shock and Vibration Digest*, vol. 20, no. 5, pp. 3–13, 1988.

[10] H. Öz, M. Pakdemirli, and E. Özkaya, "Transition behaviour from string to beam for an axially accelerating material," *Journal of Sound and Vibration*, vol. 215, no. 3, pp. 571–576, 1998.

[11] R. Parker, "Supercritical speed stability of the trivial equilibrium of an axially-moving string on an elastic foundation," *Journal of Sound and Vibration*, vol. 221, no. 2, pp. 205–219, 1999.

[12] H. Öz and M. Pakdemirli, "Vibrations of an axially moving beam with time-dependent velocity," *Journal of Sound and Vibration*, vol. 227, no. 2, pp. 239–257, 1999.

[13] V. Kartik and J. Wickert, "Vibration and guiding of moving media with edge weave imperfections," *Journal of Sound and Vibration*, vol. 291, no. 1, pp. 419–436, 2006.

[14] J. Wickert, "Non-linear vibration of a traveling tensioned beam," *International Journal of Non-Linear Mechanics*, vol. 27, no. 3, pp. 503–517, 1992.

[15] F. Pellicano and F. Zirilli, "Boundary layers and non-linear vibrations in an axially moving beam," *International Journal of Non-Linear Mechanics*, vol. 33, no. 4, pp. 691–711, 1998.

[16] G. Chakraborty and A. Mallik, "Non-linear vibration of a travelling beam having an intermediate guide," *Nonlinear Dynamics*, vol. 20, no. 3, pp. 247–265, 1999.

[17] H. Öz, M. Pakdemirli, and H. Boyacı, "Non-linear vibrations and stability of an axially moving beam with time-dependent velocity," *International Journal of Non-Linear Mechanics*, vol. 36, no. 1, pp. 107–115, 2001.

[18] L.-Q. Chen and X.-D. Yang, "Steady-state response of axially moving viscoelastic beams with pulsating speed: comparison of two nonlinear models," *International Journal of Solids and Structures*, vol. 42, no. 1, pp. 37–50, 2005.

[19] K. Marynowski, *Dynamics of the axially moving orthotropic web.* Springer Science & Business Media, 2010, vol. 38.

[20] W. Van Horssen and S. Ponomareva, "On the construction of the solution of an equation describing an axially moving string," *Journal of sound and vibration*, vol. 287, no. 1, pp. 359–366, 2005.

[21] N.-H. Zhang and L.-Q. Chen, "Nonlinear dynamical analysis of axially moving viscoelastic strings," *Chaos, Solitons & Fractals*, vol. 24, no. 4, pp. 1065–1074, 2005.

[22] M. H. Ghayesh, "Nonlinear transversal vibration and stability of an axially moving viscoelastic string supported by a partial viscoelastic guide," *Journal of Sound and Vibration*, vol. 314, no. 3, pp. 757–774, 2008.

[23] L.-Q. Chen, "A computation method for nonlinear vibration of axially accelerating viscoelastic strings," *Applied mathematics and computation*, vol. 162, no. 1, pp. 305–310, 2005.

[24] N.-H. Zhang, "Dynamic analysis of an axially moving viscoelastic string by the galerkin method using translating string eigenfunctions," *Chaos, Solitons & Fractals*, vol. 35, no. 2, pp. 291–302, 2008.

[25] L.-Q. Chen, W.-J. Zhao, and J. W. Zu, "Transient responses of an axially accelerating viscoelastic string constituted by a fractional differentiation law," *Journal of Sound and Vibration*, vol. 278, no. 4, pp. 861–871, 2004.

[26] R. Sundaram and R. C. Benson, "Tape dynamics following an impact," *Magnetics, IEEE Transactions on*, vol. 26, no. 5, pp. 2211–2213, 1990.

[27] C. Doignon and D. Knittel, "A structured light vision system for out-of-plane vibration frequencies location of a moving web," *Machine vision and applications*, vol. 16, no. 5, pp. 289–297, 2005.

[28] Y. Watanabe, S. Suzuki, M. Sugihara, and Y. Sueoka, "An experimental study of paper flutter," *Journal of fluids and Structures*, vol. 16, no. 4, pp. 529–542, 2002.

[29] D. Nguyen, "Method and apparatus for detecting amplitude and frequency of web flutter using infrared optical sensor," Dec.17 1991, a US Patent US 5,073,714.

[30] H. A. Wells, "Method of paper tension control to maintain flutter within a predetermined range," Feb.26 1985, a US Patent 4,5016,42 A.

[31] R. Ahola, "Procedure for analyzing reciprocating motion," Jan.20 1987, a US Patent 4,637,727.

[32] A. Seshadri and P. R. Pagilla, "Web flutter measurement sensor," *IEEE Sensors Journal*, vol. 7, no. 9, pp. 834–835, 2009.

[33] Y. Chang and P. Moretti, "Flow-induced vibration of free edges of thin films," *Journal of fluids and structures*, vol. 16, no. 7, pp. 989–1008, 2002.

[34] S. Stanley, A.Kilpatrich, "Method and system for measuring sheet flatness," Nov.21 1972, a US Patent US3703097A.

[35] D. Nguyen, "Apparatus for determining amplitude and frequency of web flutter," Nov.6 1990, uS Patent 4,968,386.

[36] Y. M. Luo, L. Chevalier, and E. Monteiro, "Basis for viscoelastic modelling of polyethylene terephthalate (pet) near tg with parameter identification from multiaxial elongation experiments," *International journal of material forming*, vol. 7, no. 3, pp. 359–367, 2014.

[37] L. Figiel and C. P. Buckley, "On the modelling of highly elastic flows of amorphous thermoplastics," *International Journal of Non-linear Mechanics*, vol. 44, no. 4, pp. 389–395, 2009.

[38] D. T. Films, "Physical-thermal properties," *Data sheet*, pp. 1–6, 2003.

[39] Y. Wu, W. Zhao, and J. Zhu, "A numerical approach for analyzing the transverse vibrations of an axially moving viscoelastic string," *International Journal of Modeling, Simulation, and Scientific Computing*, vol. 5, no. 03, p. 1450005, 2014.

[40] M. Pakdemirli, A. G. Ulsoy, and A. Ceranoglu, "Transverse vibration of an axially accelerating string," 1994.

[41] D. G. Stephens, "Investigation of air damping of circular and rectangular plates, a cylinder and sphere," *National aeronautics and space administration*, pp. 0–4.

[42] W. E. Baker, W. E. Woolam, and D. Young, "Air and internal damping of thin cantilever beams," *International Journal of Mechanical Sciences*, vol. 9, no. 11, pp. 743–766, 1967.

[43] L. Chen, "On galerkin discretization of axially moving nonlinear strings," *Acta Mechanica Solida Sinica*, vol. 22, no. 4, pp. 369–376, 2009.

[44] C. L. W. Jun, "Bifurcation in transverse vibration of axially accelerating viscoelastic strings," *Acta Mechanica Solida Sinica*, vol. 1, p. 013, jun2005.

[45] F. Archibald and A. Emslie, "The vibration of a string having a uniform motion along its length," *ASME Journal of Applied Mechanics*, vol. 25, no. 3, pp. 347–348, 1958.

[46] H. Gottlieb, "Non-linear vibration of a constant-tension string," *Journal of sound and vibration*, vol. 143, no. 3, pp. 455–460, 1990.

[47] P. Sensors, "Displacement measurement systems mdms, mcdms and microdms," *Manual*, pp. 0–28, 2015.

[48] P. sensors, "A usb powered fiberoptics displacement sensor model microdm-src100," *Manual*, pp. 0–4, 2015.

APPENDIX

Simplifying equation (4.15) by taking each term individually as follows:

$$1 \Rightarrow \rho A\delta \int_0^L \int_{t_1}^{t_2} v^2 dxdt$$

$$\rho Av^2 \int_{t_1}^{t_2} \int_0^L \delta dxdt = \rho Av^2 \int_{t_1}^{t_2} x\Big|_{x=0}^{x=L} dt$$

$$2 \Rightarrow \rho A\delta \int_0^L \int_{t_1}^{t_2} w_{,t}^2 \, dxdt$$

$$\rho A\delta \int_0^L \int_{t_1}^{t_2} w_{,t}^2 \, dxdt = \rho A\delta \int_0^L \int_{t_1}^{t_2} w_{,t} \, w_{,t} \, dxdt$$

$$\rho A\delta \int_0^L \int_{t_1}^{t_2} w_{,t}^2 \, dxdt = \rho A\delta \int_0^L \left(\int_{t_1}^{t_2} w_{,t} \, w_{,t} \, dt \right) dx$$

$$\rho A\delta \int_0^L \int_{t_1}^{t_2} w_{,t}^2 \, dxdt = \rho A \int_0^L \left(w_{,t} \, \delta w\Big|_{t_1}^{t_2} - \int_{t_1}^{t_2} w_{,tt} \, \delta w dt \right) dx$$

. As there is no variation in w between t_1 and t_2 , so it is equal to zero.

$$\rho A\delta \int_0^L \int_{t_1}^{t_2} w_{,t}^2 \, dxdt = -\rho A \int_{t_1}^{t_2} \left(\int_0^L w_{,tt} \, \delta w dx \right) dt$$

$$3 \Rightarrow \rho Av^2\delta \int_0^L \int_{t_1}^{t_2} w_{,x}^2 \, dxdt$$

$$\rho A v^2 \delta \int_0^L \int_{t_1}^{t_2} w_{,x}^2 \, dxdt = \rho A v^2 \delta \int_0^L \int_{t_1}^{t_2} w_{,x} \, w_{,x} \, dxdt$$

$$\rho A v^2 \delta \int_0^L \int_{t_1}^{t_2} w_{,x}^2 \, dxdt = \rho A v^2 \delta \int_{t_1}^{t_2} \left(\int_0^L w_{,x} \, w_{,x} \, dx \right) dt$$

$$\rho A v^2 \delta \int_0^L \int_{t_1}^{t_2} w_{,x}^2 \, dxdt = \rho A v^2 \int_{t_1}^{t_2} \left(w_{,x} \ \delta w \Big|_{x=0}^{x=L} \int_0^L w_{,xx} \, \delta w dx \right) dt$$

$$4 \Rightarrow 2\rho A v \delta \int_{t_1}^{t_2} \int_0^L w_{,t} \, w_{,x} \, dxdt$$

$$2\rho A v \delta \int_{t_1}^{t_2} \left(\int_0^L w_{,t} \, w_{,x} \, dx \right) dt = 2\rho A v \int_{t_1}^{t_2} \left(w_{,t} \ \delta w \Big|_{x=0}^{x=L} - \int_0^L w_{,tx} \, \delta w dx \right) dt$$

$$5 \Rightarrow \delta P \int_0^L \int_{t_1}^{t_2} w_{,x}^2 \, dxdt$$

$$\delta P \int_0^L \int_{t_1}^{t_2} w_{,x}^2 \, dxdt = \delta P \int_0^L \int_{t_1}^{t_2} w_{,x} \, w_{,x} \, dxdt$$

$$\delta P \int_0^L \int_{t_1}^{t_2} w_{,x}^2 \, dxdt = \int_{t_1}^{t_2} \left(P w_{,x} \ \delta w \Big|_{x=0}^{x=L} - P \int_0^L w_{,xx} \, \delta w dx \right) dt$$

$$6 \Rightarrow \delta E A \int_{t_1}^{t_2} \int_0^L \frac{1}{4} w_{,x}^4 \, dxdt$$

$$\delta E A \int_{t_1}^{t_2} \int_0^L \frac{1}{4} w_{,x}^4 \, dxdt = \delta E A \int_{t_1}^{t_2} \int_0^L \frac{1}{2} w_{,x}^4 \, \frac{1}{2} w_{,x}^4 \, dxdt$$

$$\delta E A \int_{t_1}^{t_2} \int_0^L \frac{1}{4} w_{,x}^4 \, dxdt = \delta E A \int_{t_1}^{t_2} \left(\int_0^L \frac{1}{2} w_{,x}^4 \, \frac{1}{2} w_{,x}^4 \, dx \right) dt$$

$$\delta E A \int_{t_1}^{t_2} \int_0^L \frac{1}{4} w_{,x}^4 \, dxdt = \delta E A \int_{t_1}^{t_2} \left(\int_0^L \frac{1}{4} w_{,x}^2 \, w_{,x}^2 w_{,x}^2 dx \right) dt$$

$$\delta E A \int_{t_1}^{t_2} \int_0^L \frac{1}{4} w_{,x}^4 \, dxdt = \delta E A \int_{t_1}^{t_2} \left(\frac{1}{4} w_{,x}^2 \, w_{,x} \, \delta w \Big|_{x=0}^{x=L} - \int_0^L \left(\frac{1}{4} w_{,x}^2 \, w_{,x} \right)_x \delta w dx \right) dt$$

VITAE

- **Personal Details:**
  - Name: Murad Ali
  - Nationality: Pakistan
  - Date of Birth: 18^{th} March, 1988
  - Email: *engrali101@gmail.com*
  - Permenant Address: Maneri Payan, Swabi, Khyber Pukhtoonkhwa, Pakistan
- **Publications:**
  - Transverse vibrations of moving web using displacement sensor (In progress)
  - Dynamics analysis of an axially moving web using displacement sensor (In progress)
  - Murad Ali, M. Hawwa "Application of Pole Placement Control to Double Inverted Pendulum(DIP) for the enhanced stability and linear response" (Poster presentation accepted at MEPEC 2015, Bahrain)
- **Education:**
  1. Bachelor of Science, University of Engineering and Technology Peshawar, Pakistan. Graduated August 2011
- **Short Synopses:** MURAD ALI is a graduating student of Mechanical Engineering Department at King Fahd University of Petroleum and Minerals (KFUPM). His CGPA at KFUPM Mechanical Engineering Department is 3.68/4.0. During his Master thesis, he visited Massachusetts Institute of Technology (MIT) USA for one semester and performed his experimental work there in the Lab of Manufacturing and Productivity. Previously he did his B.Sc. Mechatronics Engineering from University of Engineering and Technology (UET) Peshawar, Pakistan in 2011. In the undergraduate, out of 8 semesters, he secured 1 time 1^{st} and 2 times 3^{rd} position, with a 2^{nd} position in fire fighting robotics competition.